CHALMERS

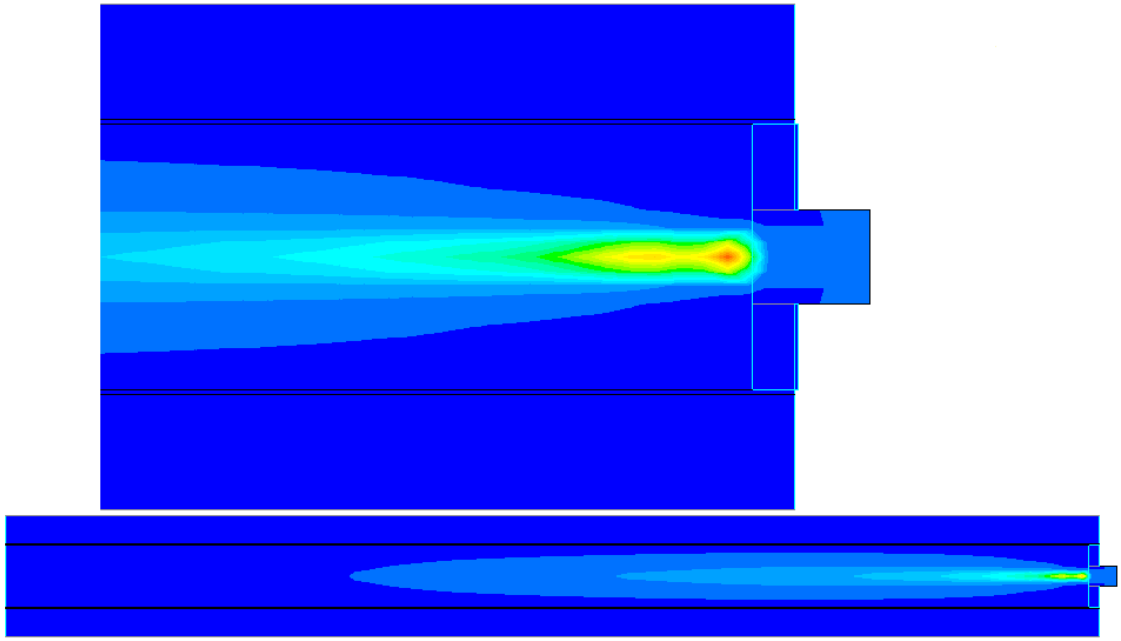

Computational Modelling of Spray Drying
With Application to Inhaled Drug Production

Master of Science Thesis

SOHEIL SOLTANI

Department of Chemical and Biological Engineering

Division of Chemical Engineering Design

CHALMERS UNIVERSITY OF TECHNOLOGY

Gothenburg, Sweden, 2012

Computational Modeling of Spray Drying

With Application to Inhaled Drug Production

SOHEIL SOLTANI

Examiner:
Professor Anders Rasmuson

Master of Science Thesis

Department of Chemical and Biological Engineering
CHALMERS UNIVERSITY OF TECHNOLOGY
Gothenburg, Sweden 2012

Computational Modeling of Spray Drying
With Application to Inhaled Drug Production
SOHEIL SOLTANI

Department of Chemical and Biological Engineering
Chalmers University of Technology
SE-412 96 Göteborg
Sweden
Telephone + 46 (0)31-772 1000

Cover: Concentration distribution of ethanol inside the dryer, see chapter 5.2 page 32.
Göteborg, Sweden 1999

Abstract

Producing fine powder is of utmost importance in respiratory drug delivery in order to make the drug respirable and permeable through the lung cell membrane. Spray drying has been used as an efficient technique; however, traditional designs for spray dryers have turned out to be improper for processing very fine particles, since unwanted phenomena like wall deposition and agglomeration of particles adversely affect the quality of the product [1]. This has been the motivation for seeking novel designs, satisfying the product requirements. One possible design has been investigated by Gerde et al. [2], in which the drying agent was separated from the moisture containing material by using a vapor permeable membrane. Furthermore, a novel technique has been utilized for injecting particles into the drying chamber. The scope of this research is then to investigate the characteristics of such a design, to develop a suitable model for that, and to use the model in order to further optimize the performance of the design.

Acknowledgement

I would like to sincerely thank Professor Anders Rasmuson for extremely valuable hints and very interesting discussions during the thesis work.

I am also thankful to Dr. Per Gerde and Dr. Fernando Acevedo from Inhalation Sciences Sweden AB, who provided me with important and practical information about the equipment.

I also appreciate the kindness and support from all my colleagues at the department of Chemical and Biological Engineering and from all my fantastic friends at Chalmers.

Last but not least, my mother and my lovely sister for their endless love, thank you and I love you both.

Finally, I would like to dedicate this thesis to the memory of my father, Prof. Dr. Fereidoun Soltani.

Table of contents

1. Introduction 9
1.1 Background 9
1.2 Scope of the work 9
1.3 Thesis outline 10
2. Case description 10
2.1 The column 10
2.2 Injection system 11
2.3 Materials and methods 13
2.3.1 Solvents 13
2.3.2 Operating conditions 13
3. Modeling approach 14
3.1 Coupling between the phases 14
3.2 Particle-particle interactions 14
3.3 Choice of a suitable model 15
3.4 Eulerian-Lagrangian models 15
3.4.1 Discrete Parcel Method (DPM) 18
3.4.2 Hydrodynamic forces on the particles 19
3.5 Particle tracking 20
3.5.1 Droplet evaporation 20
3.5.2 Droplet momentum transfer 21
3.5.3 Droplet heat transfer 21
3.6 Mass transfer through the porous membrane 21
3.6.1 Diffusivity in the gaseous mixture 23
3.6.2 Porous zone definition 24
3.7 User's Defined Function (UDF) 24
4. Simulation 25
4.1 Geometry 25
4.2 Grid generation 26
4.3 Solution 27
4.3.1 Flow regime 27
4.3.2 Boundary condition 27
4.3.2.1 Swirl inflow 28
4.3.2.2 Drying air inflow 28

4.3.2.3 Outlet 28
4.3.2.4 Temperature 28
4.3.2.5 Discrete phase 28
4.3.2.6 Porous zone 28
4.3.3 Injection system 28
4.3.4 Numerical considerations 29
4.3.4.1 Pressure-velocity coupling 29
4.3.4.2 Sequential solution algorithm 30
4.3.4.3 Grid resolution 30
4.3.4.4 Discretization schemes 30
4.3.5 Particle tracking 31
5. Results and discussion 33
5.1 Flow field 33
5.2 Particle tracking data 34
5.3 Solution quality 37
5.3.1 Validation 37
5.3.2 Convergence 40
5.3.3 Grid dependency 41
5.4 Design parameters 43
5.4.1 Swirl flow rate 44
5.4.2 Injection flow rate 45
5.4.3 Effective diffusivity of the membrane 47
6. Development of an alternative design 48
7. Conclusions 50
7.1 Summary 50
7.2 Potentials for future work 51
8. Nomenclature 51
Appendix 55
A.1 Volume fraction of the dispersed phase 55
A.2 User's Defined Function 56
References 57

1. Introduction

1.1 Background

Spray drying is a popular unit operation for processing dry powder of solid material. It has been particularly used in pharmaceutical and food industry, mostly because of the fact that the residence time of the solid material inside the dryer is short, and this is a great advantage with the case of temperature sensitive materials. Furthermore, the shape of the final product, that is solid powder, is the desired one in the aforementioned industrial applications. As discussed by Sommerfeld et. al. investigation of spray drying specification can be made considering two important categories, namely product quality and process requirement [3]. In the former one, prediction of particle size distribution (PSD), dry state of the final product as well as the occurrence of phenomena like agglomeration are of interest. Regarding process requirements, up scaling, evaluation of alternative designs and preventing wall deposition, etc. are important. Consequently, studying the performance of spray dryers with regard to the above mentioned factors has received more and more attention during the past decades.

Traditionally, spray dryer models include the overall material and energy balances with some kind of empirical drying models for the droplets. As such, the model treats the dryer as a ‘black box ‘, where no details of the important phenomena taking place inside the dryer is obtained. Such models are not able to predict the occurrence of wall deposition, PSD, agglomeration, etc., and they are of limited value for up scaling applications.

The first attempt to investigate the details of spray drying processes was made by C. T. Crowe in his famous article in 1977, in which the foundations of the Particle Source in Cell model (PSI-Cell) are introduced [4]. The central idea in this model is the coupling effect between momentum, heat and mass transfer, which distinguishes between the traditional and new modeling approaches. In traditional models, the drying agent was assumed to remain unaffected during the drying of the particles. This, as discussed by Crowe, lacks physical relevance due to the fact that the transport phenomena are coupled between the particulate and the continuous phase. Temperature of the drying medium undergoes changes as a result of heat transfer to the particulate phase. Evaporation of the particles increases the vapor concentration as well as the total mass of the continuous phase, while hydrodynamic transport of the particles through the drying chamber depletes the momentum of the continuous phase. These coupling effects give rise to the profiles of concentration, temperature, velocity and pressure within the continuous phase.

As becomes clear from the discussion above, a versatile model must be able to account for the coupling effects on the carrier phase as well, and this is the main motivation for the choice of the modeling approach in the present study. This issue will be further discussed in more detail in section 3.

1.2 Scope of the work

The main goal of this project is to obtain a model for the equipment, which can satisfactorily reproduce the experimental data. The next step would be to use the derived model in order to predict the equipment performance under different operating conditions and then further

optimize it. Finally, risk analysis should also be performed to identify the conditions which can give rise to quality loss in the final product.

1.3 Thesis outline

In the following sections, specifications of the current case are outlined, followed by the details of the modeling approach, results and discussion. Finally, the potentials for future work are also discussed.

2. Case description

2.1 The column

Physically, the dryer consists of two regions separated by a perforated tube, which form an annulus together. The droplets are injected in the inner region, and the drying air flows counter currently in the outer region. In order to facilitate both the motion of the droplets and mass transfer, additional air flow is introduced in the inner region with a swirl flow. This swirl flow plays an important role on the phenomena taking place in the inner column. It has a great impact on wall deposition, residence time distribution, agglomeration, etc. The gas diffuser which produces the swirl flow contains 40 holes; each having a diameter of $1.5mm$, and the inflow pipe forms an angle with the column wall. Figure 2.1 shows the dismantled view of the top lid of the column and makes the diffuser visible. As indicated in figure 2.1, decomposition of the inlet velocity into tangential and radial components can be done by measuring the angle of the inflow stream.

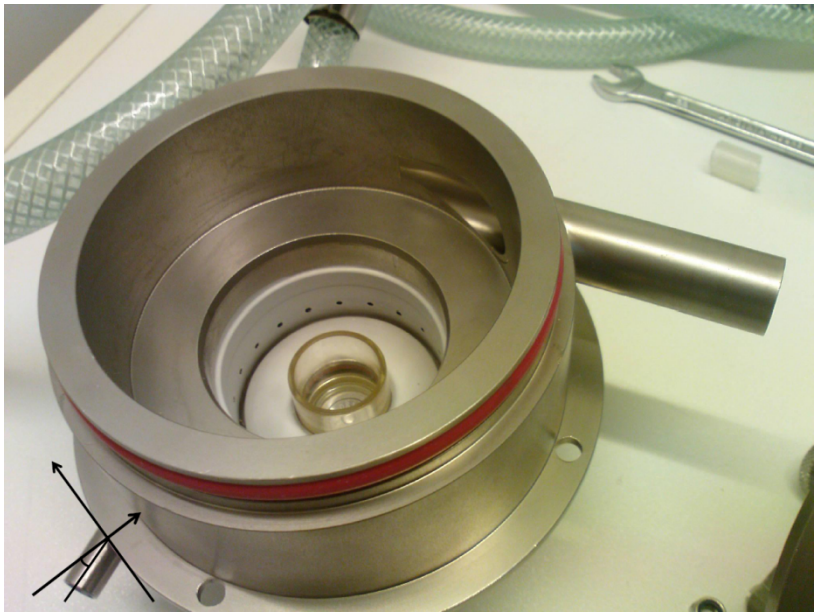

Figure 2.1. Dismantled lid of the column

The perforated tube, as shown in figure 2.2, has around 50% hole area, and its outer surface is covered with a vapor permeable membrane, which is ‘rice paper’ in this case. The vapor phase from the solvent diffuses through the membrane and further to the outer column, where

the drying air takes it out of the dryer. Properties of the membrane are discussed in more detail in 3.6.

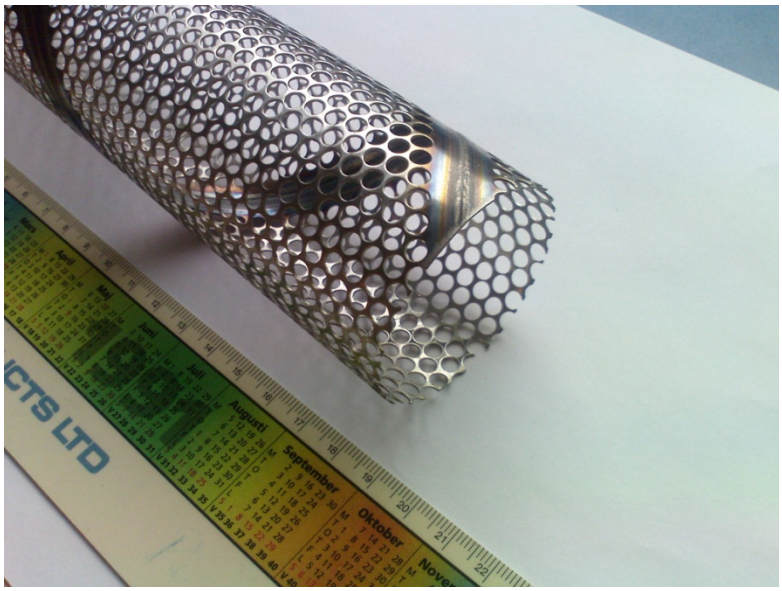

Figure 2.2. Perforated tube

2.2 Injection system

Producing fine particles suitable for inhalation strongly depends on the initial PSD. The current design utilizes Aeroneb Pro mesh nebulizer, which works based on the action of a piezoelectric actuator. Figure 2.3 show the cross sectional image of the nebulizer. The piezoelectric device is connected to an aperture plate containing micron sized holes. The diameter of the plate is only $3.5mm$, and it contains over 1000 tiny holes. Frequency of actuation is more than 100 kHz, and during each pulse, the aperture plate is displaced $1\ \mu m$ [5]. As a result of stretching and release of the aperture plate, a mist of fine droplets is continuously formed, containing droplets of $< 4\ \mu m$ in diameter on average. Figure 2.4 shows the mechanism of producing droplets in mesh nebulizers. PSD is initially tight, and the particles can be assumed to be monodispersed.

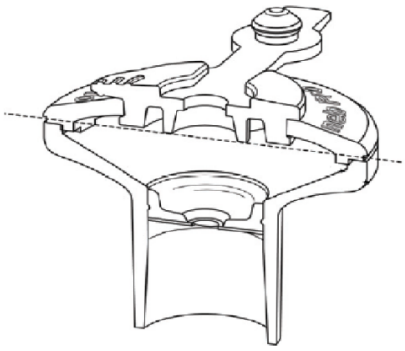

Figure 2.3. Aeroneb Pro mesh nebulizer [6]

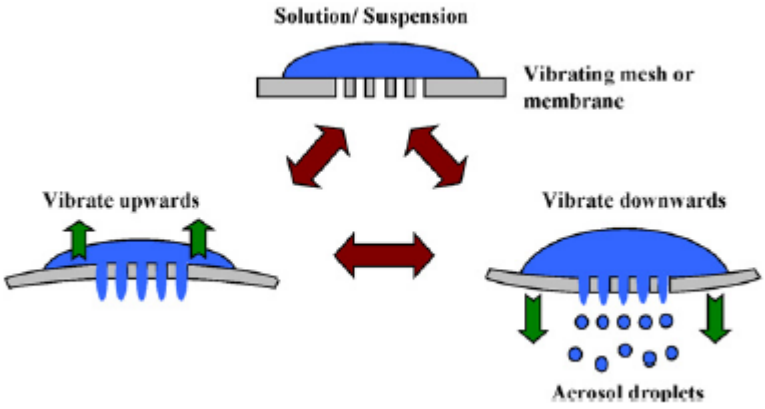

Figure 2.4. Operational mechanism of mesh nebulizers [1]

The scanning electron microscope (SEM) image of the final product is shown in figure 2.5, which also indicates a rather monodispersed PSD. Measurements show that the final product has an average diameter of around $4.7\ \mu m$, which is very close to the initial size. Figure 2.6 shows the measurement data of the aerodynamic diameter of spray dried lactose following re-aerosolization of the powder with the dustgun aerosol technology [7]. The generated aerosol was sized on a marple cascade impactor [8].

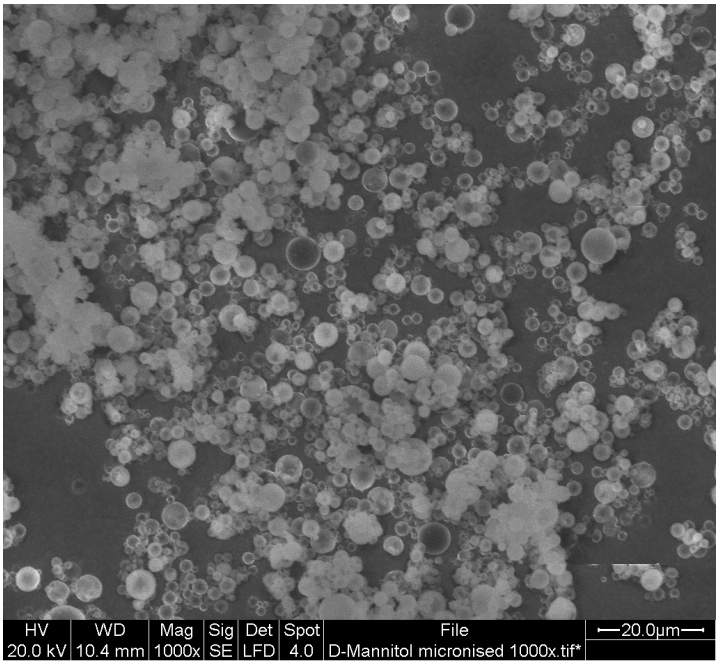

Figure 2.5. SEM image of a typical spray-dried product

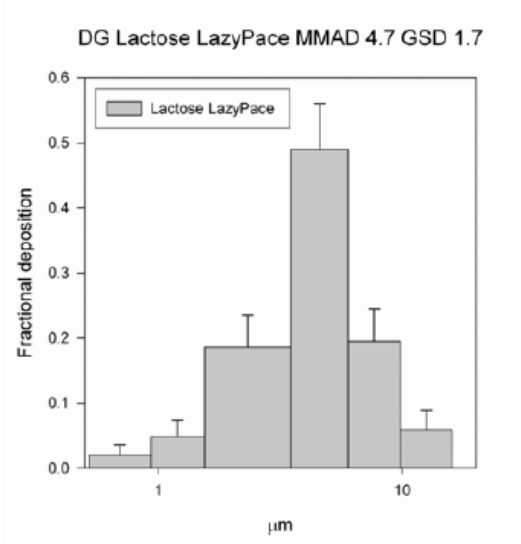

Figure 2.6. Measurement data of the aerodynamic diameter of spray dried lactose [7], [8]

2.3 Materials and methods

2.3.1 Solvents

Solvents being used in this particular application are often ethanol and water. Practical experience with ethyl acetate reveals that noticeable wall deposition occurs at the upper region of the column, while this is not the case with ethanol or water. A possible explanation of that could be related to the more volatile properties of ethyl acetate. Since there is significant swirl flow at the upper region of the column, as clearly discussed by Langrish et al., rapid evaporation of solvent reduces the momentum of small particles substantially. As a result, they fail to escape from the swirl region and will be carried to the wall by the effect of the air stream [9]. Due to its higher volatility compared to water, ethanol has been chosen as the basis for simulations. The experimental data to be used for validation are based on evaporation of pure solvents, so the simulations in the present study focus only on pure solvent without any dissolved material.

2.3.2 Operating conditions

Typical flow rates are mentioned in table 2.1 for both solvents. The significant difference between the cases is the swirl flow rate, which is much lower if ethanol is used. The reason for that is the higher volatility of ethanol.

Parameters	**Solvent**	
	Ethanol	*Water*
Drying air flow rate (L/min)	41.13	41.88
Swirl flow rate (L/min)	0.454	2
Injection initial velocity (m/s)	0.94	0.94
Injection flow rate (kg/s)	1.625E-07	2.57E-07
Temperature (K)	295	295
Pressure (Pa)	101325	101325

Table 2.1. Data for operating conditions of the dryer

3. Modeling approach

As discussed in 1.1, simplified models for droplet drying assume uniform flow, temperature and concentration field inside the drying chamber. Langrish has reviewed the detailed form of the governing equations in this framework [10]. The assumption of uniformity, however, rarely occurs in practice, which requires more rigorous models describing gradual changes in the field properties. The result is known as the finest-scale modeling, which uses computational fluid dynamics (CFD) as a tool for simulating the coupled behavior of the transport phenomena [10]. It is therefore worthwhile to investigate the coupling between the continuous and particulate phase in more detail.

3.1 Coupling between the phases

From a hydrodynamic point of view, Stokes number (St) is a measure of the degree of coupling between the phases. Stokes number is defined as the ratio between particle relaxation time and the time scale of the changes in the flow field:

$$St = \frac{\tau_{xp}}{\tau_f} \tag{3.1}$$

As such, for St<<1 the phases can be considered to be one-way coupled. In this case, particles follow the flow completely, while the continuous phase does not feel the presence of the particles. Particle relaxation time is calculated from:

$$\tau_{xp} = \frac{\rho_p d_p^2}{18\mu_f} \tag{3.2}$$

which takes a value of $6 \times 10^{-5}(s)$ for the current case. The flow field time scale is not known a priori, but since the prevailing regime is laminar, the time scale of the changes in the flow field is expected to be much larger than the time required for the dispersed phase to respond to those changes. Hence, order of magnitude estimation indicates St<<1, and this is intuitively justified regarding the very small size of the particles.

Another important parameter which should also be considered is the volume fraction of the dispersed phase (α_d). As calculated in A.1, in this case, α_d is less than 0.1% which, together with Stokes number, can be used in order to conclude that the phases are one-way coupled in terms of hydrodynamic effects. The result has an important consequence on how the dispersed phase is treated in terms of the chosen scheme for particle tracking and will be discussed in more detail in 3.4.1.

In terms of heat and mass transfer, however, the two phases are two-way coupled, meaning that the continuous phase feels the presence of the particles, since they affect the distribution of temperature and vapor concentration in the flow field.

3.2 Particle-particle interactions

Particle-particle interactions, mainly in terms of collisions between particles, have a significant effect on the simulation results. Quantitatively, α_d is a measure of how strong mutual interactions exist and is defined as:

$$\alpha_d = \lim_{\delta V \to \delta V_0} \left(\frac{\delta V_d}{\delta V} \right) \quad (3.3)$$

where δV_0 is the size of the averaging volume which guaranties smooth variation of the averaged property, which must be much larger than the particle volume while being much smaller than the physical dimensions of the system. As such, a computational cell with a minimum volume of $4 \times 10^{-9} m^3$ can be a suitable reference for calculating α_d. Computational volumes are discussed in more detail in 4.2.

Consequently, α_d represents the fraction of the computational volume occupied by the particles, and as a rule of thumb, whenever exceeds 1% mutual interactions must be taken into account. An extreme case for the volume of the dispersed phase (δV_d) can be considered as the total volumetric flow rate of the injector times the maximum residence time of the particles in each cell which may occur in the very first cell adjacent to the injection point, where droplets have not dispersed yet. As elaborated in appendix A.1, α_d is calculated around 0.1% for the extreme case, which means that particle-particle interactions can safely be neglected. This could also have been qualitatively concluded from figure 2.5, which shows a negligible change in the size of the particles. In addition to its importance with regard to product quality, neglecting collisions substantially reduces the computational load of the model.

3.3 Choice of a suitable model

There are generally two families of *ab initio* multiphase models which are applicable for simulating the performance of spray dryers, namely Eulerian-Lagrangian (E-L) and Eulerian-Eulerian (E-E) models. A detailed description of these models can be found in [11], [3].

As clearly explained in [9] and [3], E-E models are only applicable to dense flows, where the dispersed phase can be regarded as a continuum, penetrating into the carrier phase. The key requirement for continuum assumption is that information like temperature and velocity should travel in all directions in the medium as a result of particle-particle collisions. Therefore, in such regimes, collisions play the more important role than hydrodynamic forces acting on discrete particles.

From the discussion above, it becomes clear that E-E family of models is not a suitable choice for the dilute regime of the current case, where collisions are already neglected. In what follows, E-L models as the only choice for dilute regimes are discussed in more detail.

3.4 Eulerian-Lagrangian models

The continuous phase is always modeled in the Eulerian framework, where the local instantaneous balance equation of the conserved property being transported is written on an Eulerian control volume which is fixed in the space and allows for flow through its faces. Often the integral form of the balance equations is preferred, since the required condition for writing the differential form is that the property under differentiation being continuous, which is not the case for multiphase systems including interfaces. There is no such a restriction for the integral balance equations. Interfaces can then be treated as jump conditions added to the system of balance equation, meaning that the property of interest undergoes a jump in

transition from one phase to the other. The reader is referred to [12] for a detailed study of the choice of control volume and the methods for writing the balance equation. The final result is the familiar form of the continuity, Navier-Stokes and energy equations together with the transport equation for species concentrations as written in (3.4) to (3.7) respectively:

$$\frac{\partial(\rho)}{\partial t} + \frac{\partial(\rho U_j)}{\partial x_j} = S_m \tag{3.4}$$

$$\frac{\partial(U_i)}{\partial t} + \sum_j U_j \frac{\partial(U_i)}{\partial x_j} = -\frac{1}{\rho}\frac{\partial P}{\partial x_i} + \sum_j \frac{1}{\rho}\frac{\partial(\tau_{ji})}{\partial x_j} + g_i + S_P \tag{3.5}$$

$$\frac{\partial(\rho C_p T)}{\partial t} + U_j \frac{\partial(\rho C_p T)}{\partial x_j} = k\,\frac{\partial^2 T}{\partial x_j \partial x_j} - P\frac{\partial U_j}{\partial x_j} + \tau_{kj}\frac{\partial U_k}{\partial x_j} + S_T \tag{3.6}$$

$$\frac{\partial(C_n)}{\partial t} + U_j \frac{\partial(C_n)}{\partial x_j} = \frac{\partial}{\partial x_j}\left(D_n \frac{\partial C_n}{\partial x_j}\right) + S_n \tag{3.7}$$

The first and second terms in (3.4) to (3.7) are accumulation and advection of the conserved property respectively. In the above equations, S_m, S_P, S_T and S_n are source terms, due to the presence of particles, for mass, momentum, energy and concentration respectively.

In the momentum equation, the first and second terms on the right hand side are the gradients of normal and shear stresses of the fluid and the third one represents the effect of body forces.

The first term on the right hand side of (3.6) represents conductive heat transfer with k being thermal conductivity, neglecting the effect of turbulence. The second and third terms represent the effect of expansion and viscous dissipation respectively.

The first term on the right hand side of (3.7) represents species transport due to molecular diffusion.

The Lagrangian context is applied to study the discrete particles, moving with some velocity relative to a coordinate system. The equation of motion is then written for the particles using Newton's second law. The Lagrangian family of equations for a system, neglecting rotational motion, reads [11]:

$$M = constant \tag{3.8}$$

$$F_i = \frac{d(Mu_i)}{dt} \tag{3.9}$$

$$\frac{dE}{dt} = \dot{Q} - \dot{W} \tag{3.10}$$

In the above equations, M is the total mass of the system, F is the total force acting on the system, E is the total energy of the system and $\dot{Q}$, $\dot{W}$ are net heat transfer to and net work done by the system respectively. Equations (3.9), (3.10) are Newton's second law and the first law of thermodynamics respectively. Such physical laws are written for the total mass of the system and hence are valid only when M is constant. In order to be used in drying and

evaporation, where the total mass is changing, Leibnitz's transport theorem has to be applied on a control surface covering the exterior surface of the particle and moving with its velocity. One such control surface is shown in figure 3.1. Consequently, the conservation equations are then converted to the form suitable for control volume representation, where the fluxes through the boundaries are accounted for. Details of the derivation procedure can be found in [11].

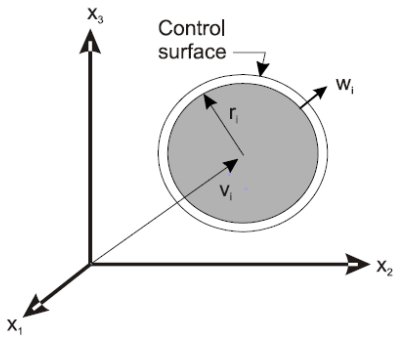

Figure 3.1. Control surface attached to the particle surface [11]

Solution to the equation of motion, (3.9), reconstructs the particle's trajectory. The central idea behind this way of modeling is that if the position of the particle is known in each time step, the local gradients of the field properties that the particle experience is then obtained from the solution of the flow field. This information is then used to calculate the changes in the particle's velocity, mass and temperature. The next step will be to calculate the counter effect of the particle on the flow field. The main role of CFD is then to solve the flow field accurately and supply the model with local information of the continuous phase.

Applied to spray drying, knowledge of the particle trajectories directly determines the amount of time each particle spends inside the chamber, which is of great importance in the case of temperature sensitive material [13].

Eulerian-Lagrangian frame of reference is very accurate, since the resolution is at the scale of discrete elements; however, it becomes computationally too heavy if applied to dense systems with too many particles. Depending on the degree of physical phenomena involved in the simulation, computers are able to handle around 100,000 particles at present. Knowing the injection flow rate and the approximate volume of each droplet, it is estimated that the number flow rate for a periodic segment[1] is around $55{,}570\ \frac{1}{sec}$. Taking into account the estimated particle residence time, as described in A.1, the total number of particles being tracked is calculated to be less than $14{,}500$ which is well below the computational limit.

The general framework described above can be further subdivided into different methods, each being suitable for particular conditions. Generally, particles are considered as 'point sources', meaning that they are assumed to have zero volume. Furthermore, bulk properties of

[1] Periodic segment is described in 4.1

the dispersed phase are calculated for the 'cloud of particles'. In order to prevent confusion regarding the variety of terminology in the E-L models, the terms suggested in [11] are used here .

One method is the so called Discrete Element Method (DEM) in which each and every individual particle is tracked at each time step. The properties of the individual particles will then determine the properties of the cloud. DEM is particularly applicable to collision dominated flows as in fluidized beds or granular flows and its advantage is that a very accurate simulation of the multiphase flow is obtained, since the resolution is at the scale of individual particles. However, in many practical situations where a large number of particles present, this method becomes computationally intractable. Alternatively, particles having the same properties, like size, velocity and temperature, can be grouped as a parcel of particles, and each parcel is then tracked at each time step. In this method, which is known as Discrete Parcel Method (DPM), the properties of the dispersed phase are calculated by ensemble averaging over the parcels being present in each computational cell [3]. As such, DPM forms the core of the modeling approach in the present study and will be discussed in more detail as follows.

3.4.1 Discrete Parcel Method (DPM)

Coupling between the two phases in terms of the transport phenomena was discussed in 3.1. In accordance to the current case where collisions are ignored, a conceptually simple technique known as the 'trajectory method' [11] can be applied, in which the particle trajectories are calculated, accounting for fluid-particle interactions. Once the trajectories are calculated, they are kept unchanged. Particles are then injected and advanced into the domain through the calculated trajectories.

The initial conditions for each trajectory j include the mass flow rate of the particles on j, $(\dot{M}_{p,j})$, as well as the starting angle and velocity of injection. Different size classes can be incorporated by using a distribution function such as Rossin-Rammler. $\dot{M}_{p,j}$ is usually assigned to each trajectory, which is then used to calculate the number flow rate:

$$\dot{N}_{p,j} = \frac{\dot{M}_{p,j}}{m_{p,j}} \qquad (3.11)$$

where $m_{p,j}$ is the initial mass of a single particle. $m_{p,j}$ and hence $\dot{N}_{p,j}$ remain constant if no agglomeration or break-up takes place.

Fundamental to the 'trajectory method' for particle tracking is that a stationary condition can be assumed. Such an assumption is fairly safe when no collision or break-up takes place in the dispersed phase. For higher orders of coupling when particle-particle interactions must also be accounted for, unsteady particle tracking must be incorporated in which no established trajectories are used, and all the parcels are tracked simultaneously at each time step. As such, variations in the particles' pathlines are also accounted for.

Regardless of either of the variants used for particle tracking, the solution algorithm at each time step starts with solving the carrier phase first. This solution is then used to track the

discrete parcels, accounting for relevant phenomena like evaporation, etc. as well. The counter effect of the dispersed phase is then reflected back into the equations of the continuous phase in terms of source terms for momentum, mass and energy. Finally, the new information of the carrier phase is used to recalculate the dispersed phase again, and this loop has to be iterated until a converged solution for both phases is obtained.

Figure 3.2 shows a comparison between the two different versions. The main advantage of the trajectory method is that a converged solution can be obtained easier, and this is of great importance as will be discussed further. Therefore, DPM in its 'trajectory method' variant is used to simulate the behavior of the particle-fluid system in the spray dryer.

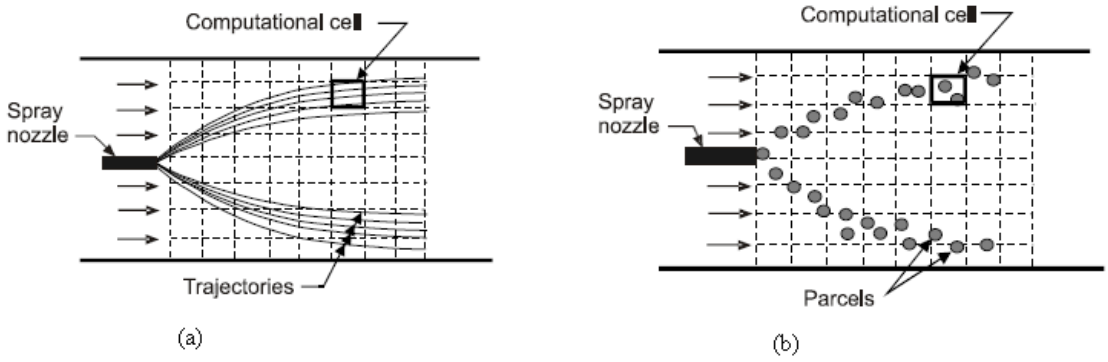

Figure 3.2. The trajectory method (a) vs. unsteady particle tracking (b) [11]

3.4.2 Hydrodynamic forces on the particles

As discussed above, knowledge of the fluid dynamic forces is crucial in formulating the equation of motion for the discrete elements. Maxey and Riley have studied the forces on individual particles in incompressible, unbounded flow field, for small spheres with translational motion and for low Reynolds numbers [14]. The resulting form of the equation of motion of the particles reads:

$$m_p \frac{d\boldsymbol{u}_p}{dt} = m_p \boldsymbol{g}_i + \oint_s \sigma_{ij} n_j dS \qquad (3.12)$$

The first term on the right hand side includes the effect of body forces, and the second one integrates the fluid stress tensor over the particle surface with n_j as the unit outward normal vector. In [12], the surface integral has been divided into two parts, distinguishing between the contributions of the undisturbed flow field and that of the disturbance flow due to the presence of the particle. As such, they have derived the forces in the Basset-Boussinesq-Oseen equation of motion for the particles, namely the drag, lift, buoyancy, Basset, added mass, Brownian and thermophoretic forces as well as the forces due to the pressure gradient.

In accordance with the present study, some of the above mentioned forces can be neglected. Assuming uniform velocity profile over the small particles, and that the particles have

irrotational motion from the beginning, lift forces become negligible. Regarding the density ratio between the continuous and discrete phase, buoyancy, Basset force as well as the added mass and pressure gradient forces are neglected. Since the particles are micron-sized, the Brownian forces are not relevant, and in the absence of severe temperature gradient in the normal direction, thermophoretic forces can also be neglected. Consequently, only gravity and the drag force are included in the equation of motion for the particles.

It is important to note that the assumptions made in the derivation approach which was pointed out above, is not consistent with most of the practical situations. For instance, the presence of other particles results in a change in the calculated drag force, which requires empirical modifications and this, can be a source of loosing precision in the modeling framework.

3.5 Particle tracking

Applying the Leibnitz's transport theorem as described in 3.4, the control volume formulation of the governing equations for the dispersed phase is obtained. These equations which form the fundamentals of transport phenomena, are introduces in this section.

3.5.1 Droplet evaporation

Considering the droplet depicted in figure 3.1, the Leibnitz's transport theorem reads:

$$\frac{dm}{dt} = -\int_{cs} \rho_s \boldsymbol{V}.d\boldsymbol{A} \qquad (3.13)$$

where m is the mass of the droplet and ρ_s, $\boldsymbol{V}$ are the fluid density and velocity with respect to the control surface respectively.

This equation can be further simplified assuming uniform distribution of velocity and the fluid density over the particle surface:

$$\frac{dm}{dt} = -\rho_s V A_d \qquad (3.14)$$

where A_d is the droplet surface area. Applying Fick's law for diffusion, one has the mass flux proportional to the concentration gradient:

$$\rho_s V \propto \frac{\rho D}{d_p}(X_s - X_\infty) \qquad (3.15)$$

where X_s, X_∞ represent the mass fraction of the droplet vapor at the droplet surface and in the bulk respectively, and D is the mass diffusivity. Assuming spherical droplet, substitution of (3.14) in (3.13) gives:

$$\frac{dm}{dt} = Sh\pi\rho D d_p(X_\infty - X_s) \qquad (3.16)$$

where the Sherwood number, Sh, is the coefficient of proportionality and in spray drying is often calculated using the Ranz-Marshall empirical correlation:

$$Sh = 2 + 0.6Re^{\frac{1}{2}}Sc^{\frac{1}{3}} \quad (3.17)\ [15]$$

Sc is the Schmidt number for the carrier phase.

3.5.2 Droplet momentum transfer

As a result of the gradual changes in the droplet's mass due to evaporation, the magnitude of the fluid dynamic forces on the particle is also changed:

$$\boldsymbol{F} = \frac{d}{dt}(m\boldsymbol{U}) = \frac{d}{dt}\int_{cv}\rho\boldsymbol{U}dv + \int_{cs}(\boldsymbol{U}+\boldsymbol{w})\rho_s\boldsymbol{V}.d\boldsymbol{A} \quad (3.18)$$

where $\boldsymbol{w}$ is the velocity of gases at the control surface with respect to the droplet's center of mass whose velocity itself is $\boldsymbol{U}$. The first term on the right hand side of (3.18) represents the accumulation of momentum inside the control volume and the second one accounts for the fluxes of momentum through the boundaries. Further expansion implementing equation (3.13) gives:

$$\boldsymbol{F} = m\frac{d\boldsymbol{U}}{dt} + \int_{cs}\boldsymbol{w}(\rho_s\boldsymbol{V}.d\boldsymbol{A}) \quad (3.19)\ [15]$$

3.5.3 Droplet heat transfer

Similar to what derived for droplet evaporation, heat transfer to the droplet can be described as follows:

$$\dot{Q}_d = Nu.k.\pi d(T_\infty - T_s) \quad (3.20)$$

with k being the thermal conductivity of the carrier phase. T_∞ and T_s are temperature of the carrier phase and the droplet surface respectively. The Nusselt number is the coefficient of proportionality and is obtained from the Ranz-Marshall correlation:

$$Nu = 2 + 0.6Re^{\frac{1}{2}}Pr^{\frac{1}{3}} \quad (3.21)\ [15]$$

Pr is the Prandtl number for the carrier phase.

3.6 Mass transfer through the porous membrane

Mass transfer can be studied separately for the gaseous phase as well as the membrane. Considering evaporation from each droplet, ethanol is being transported from the surface of the droplet to the bulk of the gaseous phase in the inner column and then further through the membrane.

The vapor permeable membrane in the system is a thin layer of the so called 'rice paper' with a measured thickness of around 50 µm. It is possible to see through the membrane, and qualitatively, it can be concluded that the characteristics of the membrane fall in the range of porous ones with rather large porosity. However, since the pressure difference over the membrane is negligible, the bulk flow through the membrane, i.e. normal to the main flow direction can be neglected. Furthermore, due to the rather large pore size of the membrane, the diffusion mechanism can be assumed as ordinary diffusion, and Knudsen mechanism can be neglected [16].

Having passed through the membrane, ethanol is diffused to the bulk of the drying air in the outer column and eventually will be taken out of the dryer.

It is important to note that the membrane is put on the perforated support tube shown in figure 2.2. Hole area of the tube is around 50%, and its thickness is 1 mm. As such, only half of the total surface area is available for diffusion, and also compared to the thickness of the membrane, it becomes important to account for mass transfer resistance of the tube as well.

The driving force for mass transfer, which is concentration difference, is calculated when the coupled equations of the flow with that of the species are being solved. The important parameter which then determines the total flux of the species is diffusivity, which in turn determines the mass transfer coefficient. Transport through the membrane can be quantified by providing the solver with an effective diffusivity for ethanol. The influencing parameters here are the porosity and tortuosity of the membrane denoted by ϵ and τ respectively:

$$D_{eff} = \frac{D.\epsilon}{\tau} \qquad (3.22)$$

Experimental determination of D_{eff} is beyond the scope of the current study, yet it requires a thorough discussion on how to estimate a reasonable value for the above mentioned parameters. Tortuosity, in particular, is very difficult to calculate accurately, since it depends on how the fibers of the paper structure are positioned. In that sense, the problem attains a random feature which makes any estimation of tortuosity vulnerable to severe uncertainty. Zbicinski has pointed out the important effect of the model parameters on the quality of the simulation results [17]. As discussed in [17], any error in the value of those parameters propagates in the model and influences the results. It then becomes clear that how important is to have a reliable value for D_{eff}, especially because it plays the key role in making a cut-off in ethanol concentration between the two outflow streams of the dryer.

In [9] the work done by Oakley et. al has been reviewed, in which a similar challenge was found with turbulence parameters. Two solutions proposed for that are either to vary the unknown parameter such that the model fits the experimental data or to calculate it from a separate simulation. In relation with the current case, the first solution has been used, starting with an initial guess for D_{eff} which is two orders of magnitude lower than the gaseous diffusivity of ethanol into air. The idea is then to integrate the effect of both the perforated tube and membrane in the value obtained for D_{eff}. From here on, they are, both together, called membrane.

Experimental data available for the column includes the measurements of the ethanol concentration at the drying air outflow as well as at the inner column's outflow, in $(\frac{\mu L\ ethanol}{m^3})$. Only the first standard case has been used in order to calculate the effective diffusivity, for which the measurements are shown in figures 3.3.

A value of $D_{eff} = 8.378 \times 10^{-6} \frac{m^2}{s}$ has been observed to fit the data reasonably well, and this value is then used in the model for further investigations. Upon substitution in (3.22), the geometric factor for the membrane can be calculated:

$$\frac{\epsilon}{\tau} = 0.51$$

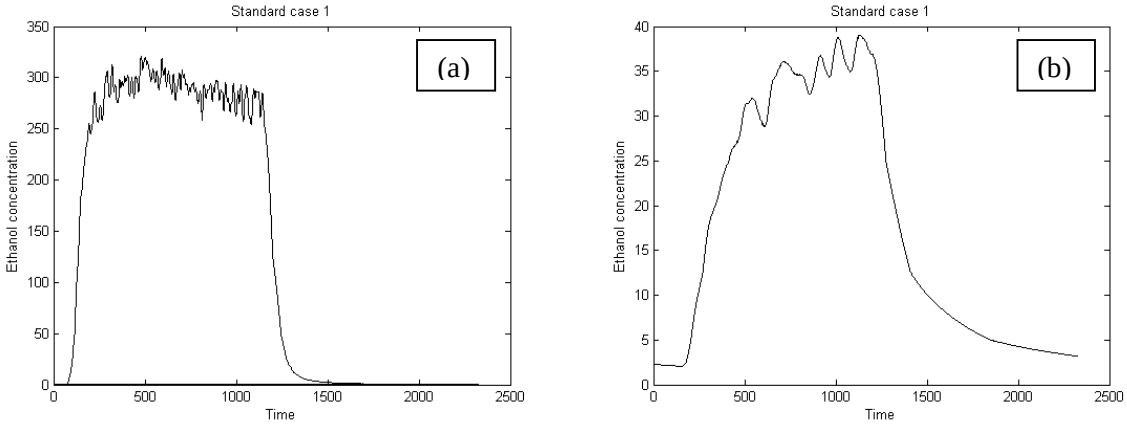

Figure 3.3. Ethanol concentration in $(\frac{\mu L}{m^3})$ vs. time $(sec.)$ at the drying air outlet (a) and the inner column outlet (b) for standard case 1

3.6.1 Diffusivity in the gaseous mixture

In order to obtain a reliable distribution of the species concentration in the system, a suitable value for diffusivity in the gaseous mixture must be supplied to the solver for all the species. Assuming that the ideal gas law is applicable to the system, the kinetic theory of gases can then be used to evaluate the diffusivity of species. Temperature dependence of diffusivity is also accounted for in the same framework using the Chapmann-Enskog equation. As a result, diffusivity is defined to vary with $T^{1.5}$.

At $295\ K$, the following values for diffusivities have been calculated:

$$D_{O_2-air} = 2.054 \times 10^{-5} \frac{m^2}{s}$$

$$D_{Ethanol-air} = 1.641 \times 10^{-5} \frac{m^2}{s}$$

$$D_{N_2-air} = 2.054 \times 10^{-5} \frac{m^2}{s}$$

$$D_{H_2O-air} = 2.564 \times 10^{-5} \frac{m^2}{s}$$

3.6.2 Porous zone definition

From the results in 3.6, the porous membrane can be characterized as follows. Assuming ideal gas law as well as identical pressure and temperature on both sides of the membrane, the trans-membrane flux of species can be described using the following equation [16]:

$$N_i = \frac{D_{ei}}{RT\Delta m}(P_{i0} - P_{iL}) \qquad (3.23)$$

This can further be related to permeability, defined as:

$$N_i = \frac{P_{Mi}}{\Delta m} \times (driving\ force) \qquad (3.24)$$

The built-in model for porous media in ANSYS FLUENT has been used to simulate mass transfer through the vapor-permeable membrane. The original model basically consists of the viscous and inertial contributions to momentum loss in the flow (the first and second terms in (3.25)). Therefore, it can be interpreted as a depleting momentum source term in the momentum equation:

$$S_i = -\left(\sum_{j=1}^{3} D_{ij}\mu V_j + \sum_{j=1}^{3} C_{ij}\frac{1}{2}\rho|V|V_j\right) \qquad (3.25)\ [18]$$

where i represents the principle directions, $|V|$ the velocity magnitude, and D_{ij}, C are prescribed parameters for viscous and inertial losses respectively. Contribution of the inertial losses can be neglected in the case of laminar flows, which reduces the model to the Darcy's law. $D_{ij}\ \mu$ in (3.25) is correlated with permeability and can be calculated using the value of the effective diffusivity obtained in 3.6:

$$D_{ij} = 1.21 \times 10^{15}\frac{1}{m^2}$$

This parameter determines the conditions of the flow through the porous medium, and such a large momentum loss indicates negligible bulk flow.

3.7 User's Defined Function (UDF)

In order to distinguish between the bulk phase and the porous zone in terms of diffusivity, a UDF has been written in C programming language. Logically, it starts with an enumerated list of species, and then for each one, different zones corresponding to the bulk phases and the porous membrane are distinguished. In the bulk zones, temperature of each and every cell is recalled and used for calculating diffusivity based on the kinetic theory of gases as described in 3.6.1. For the porous zone, the effective diffusivity obtained in 3.6 is supplied, and finally the diffusivity value is returned to the solver. The source code of the UDF is provided in appendix A.2. Figure 3.4 shows how the different regions in the column are distinguished in terms of diffusivity.

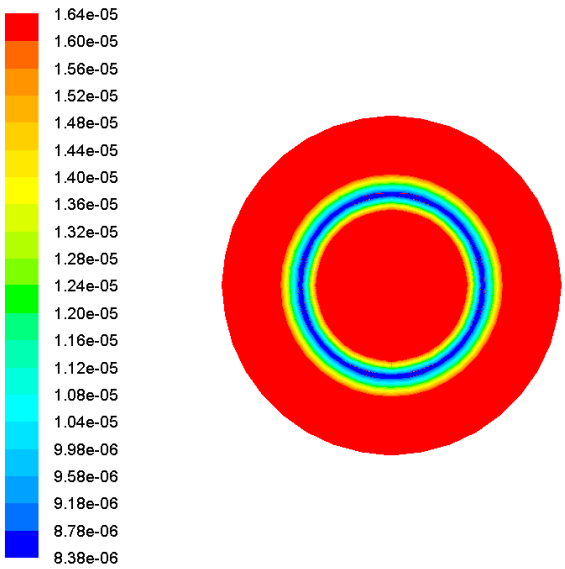

Figure 3.4. Contour plot of diffusivity value after interpreting the UDF, top-to-bottom view of the dryer projected on the XY plane

Implementing the UDF in the model will be the last step in formulating the framework of the model. The porous zone is well-defined, and the model is ready to use for obtaining results.

4. Simulation

ANSYS FLUENT has been used for this study alongside with a user defined function (UDF), written in C programming language, to account for the effective diffusivity of the membrane. The procedure of setting up a simulation starts from defining the geometry. The next step is to discretize the domain into a number of computational cells using the finite volume method. This is also known as grid generation or meshing. Numerically, the system of partial differential equations (PDEs) will then be discretized on each and every cell, such that algebraic equations are obtained. The last step is to specify the boundary conditions and other parameters of the model and eventually solve the equations. This can be followed by post processing in order to obtain more user-friendly results of the simulation. The above mentioned steps are described in the following sections.

4.1 Geometry

Dimensions of the different components of the system are as mentioned in table 4.1. An important factor is the ratio of the dryer height to its diameter. Since the significant hydrodynamic effects take place in the interior column, the corresponding diameter of 50 mm should be considered. According to this ratio, dryers are categorized into short-form and tall-form dryers [9], where the height-to-diameter ratio in the latter group is higher than 5. As such, the current design with a ratio of 17.3 is considered as tall-form, and the flow field is expected to be close to plug flow pattern in many regions.

Interior column	Exterior column	Nebulizer (the plastic mouth excluding the liquid reservoir)	Perforated tube
D = 50mm	D = 95mm	D = 18mm	Thickness = 1mm
L= 850mm	L = 850mm	L = 22mm	Hole area = 53%

Table 4.1. Physical dimensions of the dryer

Figure 4.1 shows the three dimensional geometry introduced to the model along with different components of the column. Although a full view is depicted for better visualization, only a 30^0 segment of the column is simulated due to rotational symmetry. This can significantly reduce the computational power required.

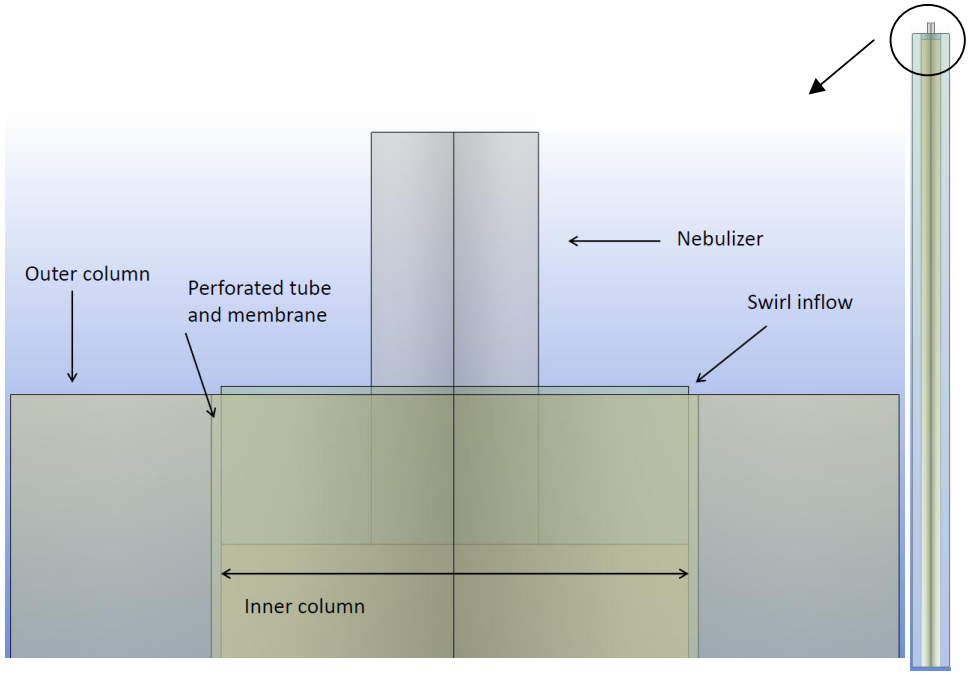

Figure 4.1. Geometry

4.2 Grid generation

ANSYS meshing platform has been used to produce the grid. A fine mesh with 6207 elements is then obtained with the details as shown in table 4.2. Aspect ratio and skewness as two important factors determining the quality of mesh have been chosen. Aspect ratio is recommended to be below 5, and skewness should be less than 0.95 maximum and less than 0.33 on average [19]. As such, the corresponding values are within the recommended ranges and well below the extreme limits on average. Such a fine mesh is desired in that it gives a smooth change in the field properties during iterations and so enhances convergence. However, maximum aspect ratio is higher than the recommended value, and local refining of the mesh can be applied on the corresponding regions.

Property	Min.	Max.	Average
Skewness	5.56E-02	0.88	0.17
Aspect ratio	1.22	9.65	2.33

Table 4.2. Details of the mesh

4.3 Solution

As described above, three families of equations have to be solved for the flow field, temperature and species concentration. These equations must be supplied with properly defined boundary conditions. Furthermore, there are a number of important numerical issues which have to be considered. These will be discussed in the following sections.

4.3.1 Flow regime

Dou et al. [20] have investigated the critical Reynolds number in annular flows using the energy gradient analysis. Accordingly, for a radius ratio around 0.5 corresponding to the design's geometry, the critical Re number is predicted to be around 2400. Calculation of the Reynolds number in the annulus part reveals a very low Re of 481. Also, in the inner part of the annulus which can be considered as a simple pipe with a transition Reynolds number of around 2100, calculated Re number is around 40 in the swirl inflow region to maximum 400 in the outlet region. As such, prevailing flow regime in the system can safely be considered as laminar everywhere.

From a numerical point of view, an important consequence of laminar regime is that the classical form of the Navier-Stokes equation is solved without applying further time averaging. The consequences of that are less computational power required, better convergence and no concern about losing precision due to averaging procedure and consequent problems with turbulence modeling and closure laws in the final results.

Apart from numerical issues, another impact of turbulence on the simulation results is the broadening effect on the probability density function (PDF) of the particle diameter [21]. Fluctuations in the local value of velocity, temperature and species concentration influences the PSD, and this has a significant effect on the product quality in the present case. Furthermore, particle size has a direct impact on particle dispersion, and this cannot be neglected regarding the importance of wall deposition.

Turbulent effects are particularly important where strong swirl flow exists, and that corresponds to the region where particles are either droplets or newly formed crystals with wet surfaces and high stickiness properties. Therefore, despite the fact that turbulence significantly enhances mass transfer, it should be avoided in this particular design, mainly due to the fact that wall deposition and agglomeration must be avoided as much as possible.

4.3.2 Boundary condition

The choice of the boundary conditions significantly affects the simulation results. Therefore, it is very important to have well defined boundary conditions with as accurate values as possible.

4.3.2.1 Swirl inflow

A plane has been defined from the top down to 0.45 mm, which simulates the gas diffuser, as depicted in figure 4.1. The thickness has been calculated such that the flow can be considered to be uniformly distributed over the plane, and that the surface area available to the flow would be equal to the total surface of the tiny holes corresponding to a 30^0 periodic segment. Each hole has a diameter of 1.5 mm, giving a total surface area of $5.89 \times 10^{-6} m^2$ for a periodic segment. The angle between the inlet pipe and the gas diffuser is around 20°, which, in cylindrical coordinate, gives two components of the inlet velocity, namely tangential and radial. The contribution of each velocity component is calculated to be -0.34 and -0.94 respectively. The negative sign determines the direction of the flow, i.e. towards the center of the cylinder and counterclockwise. The total velocity magnitude has been calculated as $0.08 \frac{m}{s}$ based on the volumetric flow rate and the calculated surface area.

4.3.2.2 Drying air inflow

Velocity inlet, normal to the boundary, has been defined with the velocity magnitude of $0.14 \frac{m}{s}$ computed from the total volumetric flow rate and the corresponding hydraulic diameter, i.e. $44\ mm$.

4.3.2.3 Outlet

If the details of the flow are not known a priori, one can choose simple 'outflow' boundary condition in the outlet. In this way, ANSYS FLUENT extrapolates the required information from inside the domain, considering no impact on the upstream flow as well as overall mass balance satisfied. This is best applied on fully developed flows, where the changes in flow properties in the axial direction are negligible. Though being simple, this type of boundary conditions does not work properly when backflow occurs at the outlet. For those situations as well as when multiple outlets are defined, the more rigorous type which is 'pressure outlet' results in better convergence, since gradients in the axial direction are also accounted for [19]. As such, the two outflows in the simulation case are defined as 'pressure outlet'.

4.3.2.4 Temperature

Temperature of the ambient as well as the inlet streams is set to $295\ K$. The outer wall as well as the porous zone is assumed to be in thermal equilibrium with the surroundings.

4.3.2.5 Discrete phase

Particles are defined to 'escape' the domain at the outlet of the column. To simulate wall deposition, discrete phase boundary condition was set to 'trap' at the corresponding walls.

4.3.2.6 Porous zone

Both the interior and exterior surfaces of the porous zone were defined as 'interior' in order to calculate the transport of the properties through.

4.3.3 Injection system

The built-in module in ANSYS FLUENT has been used to define a group injection with 85 particle streams. This number corresponds to the total number of micron-sized holes on the aperture plate, as described in 2.2, which has been calculated for one periodic segment.

Another parameter required for defining the injection is the initial injection velocity, for which experimental measurements have not been available. Regarding the variety of manufacturers and the products as well as the influence of the physical properties of the solvent, very different data has been reported in the literature. On the other hand, since measuring the injection velocity at the point where the droplets leave the nozzle is practically difficult, measurements are often performed some distance away from the nozzle. As such, the reported data represents the aerosol velocity not the injection velocity.

Eslamian et al. have measured the droplets' velocity in a setup where the particles have been under severe buoyancy force from the hot carrier gas. Injection with a vibrating mesh nebulizer (Omron Healthcare Co., NE-U22) operating at $1.8\ kHz$ was in the upward direction, and measurements have been performed at $2\ cm$ from the nozzle where an average velocity of $1.5\frac{m}{s}$ has been reported [22].

Arulmuthu et al. have used the same nebulizer as with the previous study but with an operating frequency of $175\ kHz$. Flow in each nozzle has been simulated, and the aerosol velocity has been reported approximately $1\frac{m}{s}$, measured by high speed imaging [23].

In the current study, the principle of continuity between the total flow rate and that for each nozzle has been used in order to estimate the injection velocity. Assuming that the diameter of each hole is slightly less than that of the droplets, an approximate value of $3\ \mu m$ for that gives the initial velocity around $0.94\frac{m}{s}$ which falls in the range reported in the literature.

4.3.4 Numerical considerations

From a numerical point of view, stability and accuracy of the solution are very important parameters. In this simulation, there are many coupled phenomena interacting with each other, like for example species transport in the inner column, through the membrane and in the outer column, or heat effects in the bulk flow coupled with evaporation of the droplets. These coupled phenomena increase the instability of the solution to the system of equations, and hence a robust strategy has to be organized in order to have a good control over the numerical issues. Sometimes it becomes a trade-off between accuracy and stability, meaning that a less accurate scheme is chosen in order to obtain better convergence. These aspects are discussed in more details as follows.

4.3.4.1 Pressure-velocity coupling

Velocity and pressure have a coupled interaction through the momentum equation, which itself is coupled with the continuity equation through velocity. However, since there is no term including pressure in the continuity equation, special consideration is required in order to correct the guessed value in each iteration if the equations are solved one at a time. One solution to that is to treat the system of continuity and momentum equations in a coupled manner, which means that unknown pressure and velocity components will be solved together in a matrix form. This requires more time, but the solution will be more stable, and hence a coupled scheme has been chosen for the current case.

4.3.4.2 Sequential solution algorithm

Three families of equations being solved are flow, species and energy. In order to improve stability and convergence behavior, these equations can be solved sequentially. In this way a close-to-converged solution for each family of equations is obtained before the next one is included and solved together with the previous one(s). For the excluded equations, constant values for the independent variables are assumed in each cell during iterations. As such the following procedure can be applied:

1- Solve the flow field (only the carrier phase first)
2- Introduce the dispersed phase and solve the flow field again
3- Since the physical properties of the carrier phase as well as the diffusivity values are temperature dependent, a primary distribution of temperature is obtained by solving the energy equation only, while the other equations are turned off
4- The flow field is now solved again together with the energy equation in order to adapt its properties with the calculated temperature
5- The transport equation for the species concentration can now be included and solved together with the other equations

4.3.4.3 Grid resolution

Regarding both stability and accuracy, a finer mesh generally results in a higher quality of the solution; however, this would be at the cost of increased computational time. A very coarse mesh, on the other hand, decreases the stability of the solution, because the grid resolution is not enough to capture the important details. An effective tradeoff would be to use a normal mesh on the overall domain and locally adapt it wherever higher resolution is desired.

In the current study, the fine mesh described in 4.2 has been used for the whole domain except the porous zone. Due to its very low thickness compared to the geometry dimensions, the porous zone, by default, is meshed with only one cell layer. However, since the concentration profile in this zone is calculated using the effective diffusivity, one cell layer will not be sufficient to capture the gradual changes in concentration. Therefore, the mesh has been locally adapted in this zone such that at least two cell layers are obtained in order to better calculate the concentration profile.

4.3.4.4 Discretization schemes

In finite volume method, numerical solution to a PDE includes calculating the values of the independent variable on the faces of the computational cells. The cell values are then calculated using some kind of area-weighted averaging over all the face values. Therefore, a proper discretization scheme would be required in order to calculate the face values. There are a number of possible choices for discretizing the differential terms in the balance equations. Two of the more popular ones, namely first and second order upwind schemes are considered for this case. A first order upwind scheme estimates the face value from the upwind cell:

$$\phi_f = \phi_U \qquad (4.1)$$

with subscripts f and U denoting face and the upwind cell respectively. It is clear that this scheme works well for the cells aligned with the flow direction; however, it predicts too large

values for the cells in the other directions. This drawback, which is also known as the so called 'numerical diffusion' decreases the accuracy of this scheme. Nevertheless, first order upwind is inherently bounded and hence has a very good convergence behavior. Boundedness means that the calculated value is neither smaller nor larger than the values used for calculation [19]. Numerical diffusion can be improved by choosing a finer mesh, and grid dependency of the solution must always be checked if a first order scheme is used. This issue is discussed in more detail 5.3.3.

A second order upwind scheme, on the other hand, uses two upwind cells to approximate the face value:

$$\frac{\phi_f - \phi_U}{x_f - x_U} = \frac{\phi_U - \phi_{UU}}{x_U - x_{UU}} \qquad (4.2)$$

where subscript UU denotes the second upwind cell and x is the spatial position of the cell/face centroid. As such, this method is second order accurate; however, it does not necessarily uphold boundedness which can give rise to stability problems.

Therefore, first order upwind has been chosen as the primary discretization scheme in order to obtain a more stable solution, which can further be used with a second order scheme if higher accuracy is required.

4.3.5 Particle tracking

The following settings have been applied to the solver in relation of discrete phase model. 'Interaction with the continuous phase' is activated in order to account for coupling between the phases. It is also possible to choose how many iterations in the continuous phase are performed per each iteration for the discrete phase. The value depends on the physics of the system, and in this particular case where the droplets are evaporating and causing significant changes in the concentration of the continuous phase, more iterations in the continuous phase can be recommended before the next iteration in the discrete phase is started. For the current conditions a value of 15 has performed reasonably well.

Another issue which is also of importance from a numerical point of view is how the equation of motion of the particle is treated. Mathematically, it is an ordinary differential equation with respect to time, which is coupled to the system of PDEs through the continuous phase velocity. In order to obtain a good solution in terms of both accuracy and convergence, it is important to carefully consider the so called 'time-marching' of the equation of motion. In an ideal case, the time interval chosen for time marching must be chosen as follows:

$$\Delta t = (0.3\ up\ to\ 0.5) \times \tau_{min} \qquad (4.3)$$

where τ_{min} is the smallest time scale of the system, which is normally the minimum of the following time scales:

1- Particle relaxation time
2- Time scale of collisions
3- Particle residence time
4- Integral time scale of the flow field

As such, the solution will be able to capture almost all the phenomena taking place in the particulate phase. In relation to the current case, particle relaxation time is the limiting factor, which have been approximated from (3.2) as $6 \times 10^{-5}(s)$. Practically the time interval for integrating the equation of motion can be supplied to the solver by choosing a value called 'step length factor'. The particle trajectory in each computational cell is then divided into a number of sequences equal to the supplied value, such that the time interval for each step meets the numerical requirement. It is on the other hand a tradeoff between accuracy and computational time, since the particle relaxation time it extremely low, and tracking particles on that time scale increases the computational time significantly.

If the particle encounters a recirculation region in the domain in which it is trapped for a long time, the solution procedure cannot proceed until the particle escape that region. This, however, can cause numerical problems, and therefore a limit can be defined for maximum number of time steps for integrating the equation of motion. If this limit is reached and the particle fails to escape the region, its trajectory is reported as 'incomplete'. The maximum limit in the current study is set such that all the trajectories are computed completely.

Figure 4.2 shows the graphical user's interface in which the settings mentioned above can be applied.

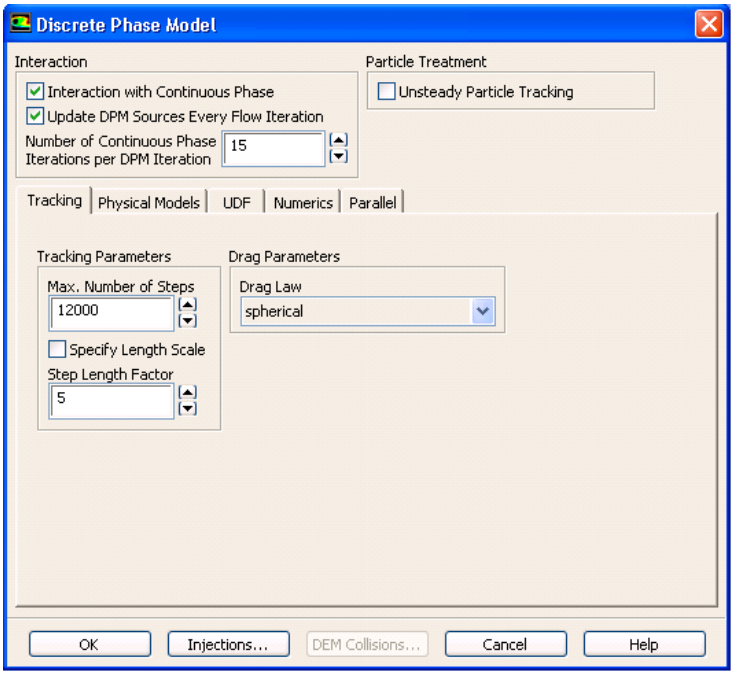

Figure 4.2. Settings for the discrete phase model

5. Results and discussion

Post processing of the simulation results has been done in both graphical and numerical formats in ANSYS FLUENT. The results are provided in this section followed by an analysis of the data obtained from the simulation. The basis for the simulation results, unless specified, is one of the standard cases for which experimental data was reported.

5.1 Flow field

The solution to the flow field is often reported as vector plots of the velocity in the domain, which can give an indication about the flow pattern in different regions. The region of highest interest is where the swirl flow dominates, which corresponds to zones with highest probability of wall deposition. Nevertheless, the swirl flow is required in order to stabilize the aerosol stream. A vector plot of the flow field is shown in figure 5.1. Data extraction from the image indicates the presence of strong swirl flow from the inlet at the top down to $15 - 20\ cm$. This is in qualitative agreement with practical experience with ethyl acetate, for which considerable amount of wall deposition has been observed. As depicted in figure 5.1, the swirl flow gradually damps out within $60\ cm$ from the top, and the flow pattern in the remaining part of the column is fairly uniform.

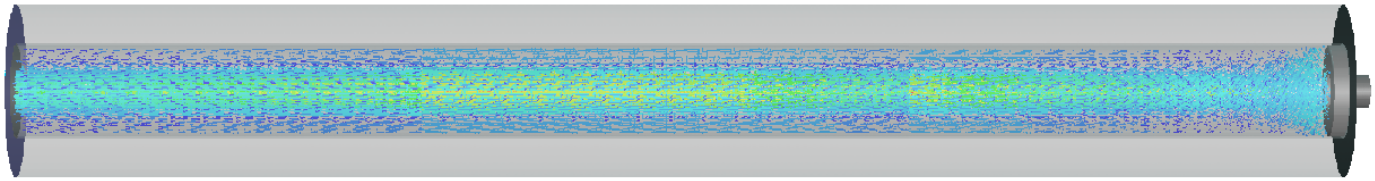

Figure 5.1. Vector plot of the flow field

Figure 5.2 shows a contour plot of the cell Reynolds number, which indicates that the assumption of laminar flow is satisfied.

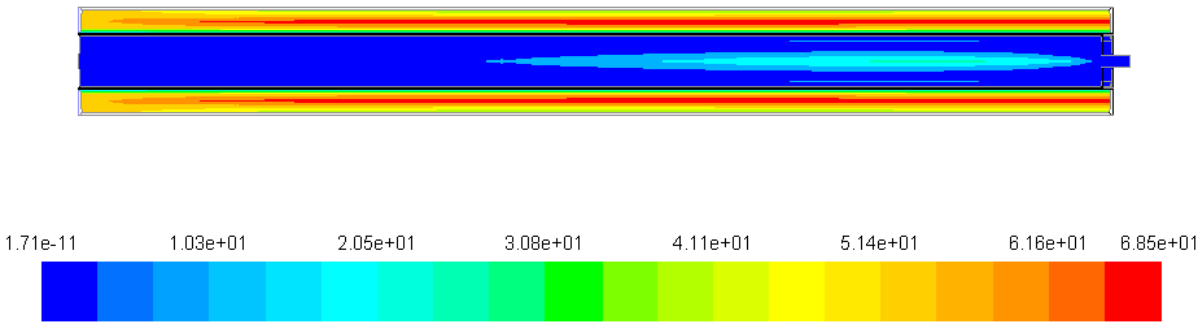

Figure 5.2. Contour plot of the cell Reynolds number

5.2 Particle tracking data

A summary of the particle tracking data is shown in table 5.1. According to table 5.1, all the trajectories are evaporated, and none of them is trapped on the wall or in a recirculating region.

		Elapsed time (s)			
Trajectory	Number	Min.	Max.	Avg.	Std. deviation
Evaporated	85	4.61e-02	1.31e-01	1.09e-01	1.43e-02
Incomplete, trapped, etc.	0				
Energy transfer summary(W)		**Sensible heat**	**Latent heat**		**Total**
		1.05e-04	1.16e-02		1.17e-02
Mass transfer summary					
Injection flow rate ($\frac{kg}{s}$)	1.35e-08				
Evaporated ($\frac{kg}{s}$)	1.35e-08				

Table 5.1. Summary of particle tracking data

Results of heat transfer are according to expectations:

$$\lambda_{Ethanol} = 855237 \frac{J}{kg} \Rightarrow$$

$$\Delta \dot{H}_{Evaporation} = 855237 \times 1.35 \times 10^{-8} = 1.16 \times 10^{-2}\ W$$

where λ is the latent heat of evaporation.

A contour plot of temperature distribution is shown in figure 5.3. Approximation of the wet bulb temperature for air-ethanol at $30^o\ C$ assuming no ethanol in the air predicts a value of $T_w = 277\ K$ [24]. Accounting for the amount of ethanol present in the surrounding air as well as the surrounding temperature of $22^o\ C$, the calculated temperature profile in figure 5.3 is in good agreement with the wet bulb temperature of the current case.

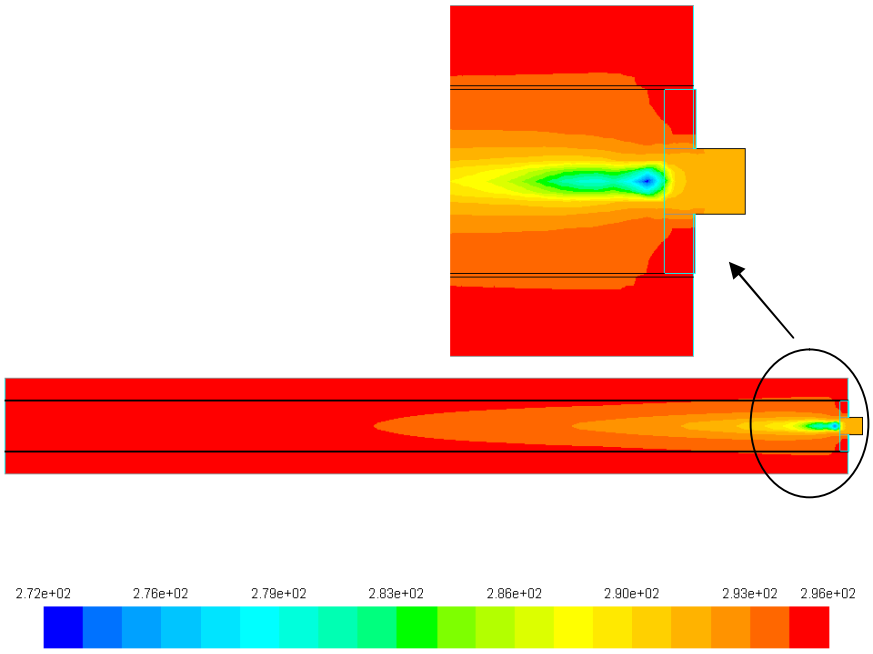

Figure 5.3 Contour plot of the distribution of temperature (K)

Figure 5.4 shows a contour plot of the distribution of ethanol concentration in the system.

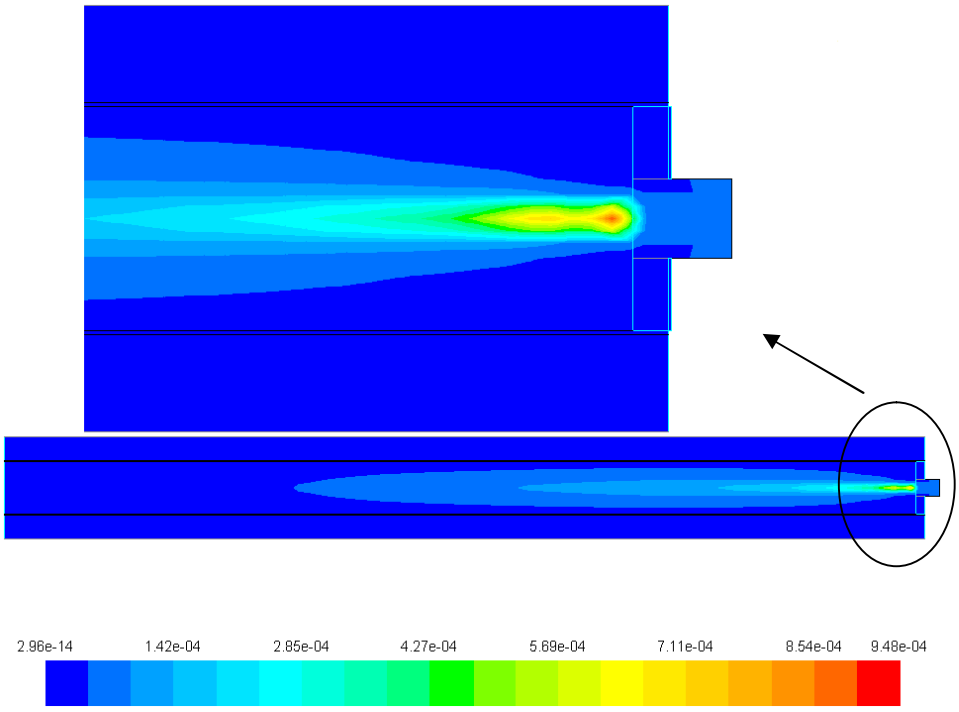

Figure 5.4 Contour plot of the distribution of ethanol concentration $\left(\frac{kmol}{m^3}\right)$

Figures 5.5a-d show some details of particle tracking data for 9 trajectories randomly selected among the total 85 ones. The blue, black and red colors correspond to the trajectories close to the centerline, intermediate and the outer most particle streams respectively.

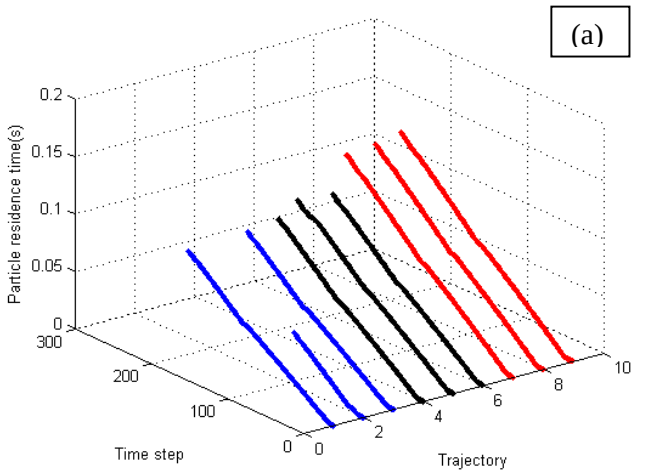

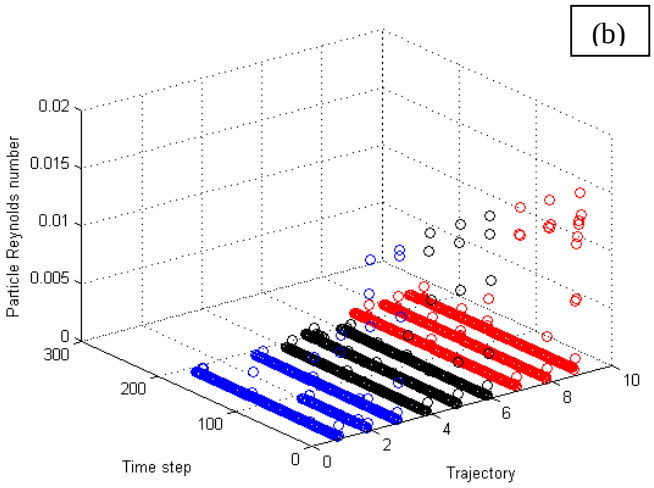

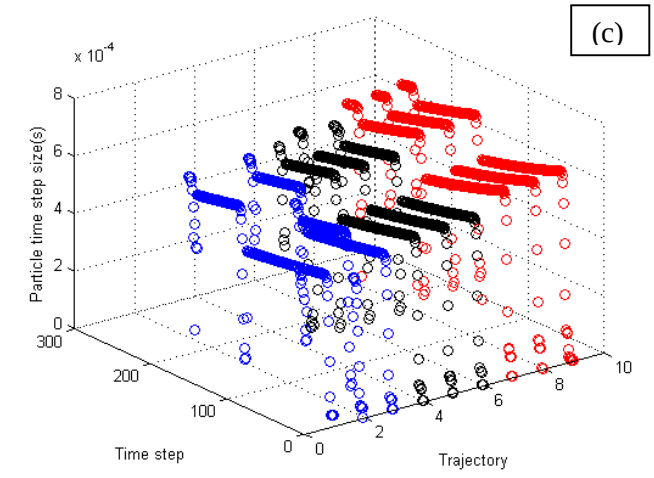

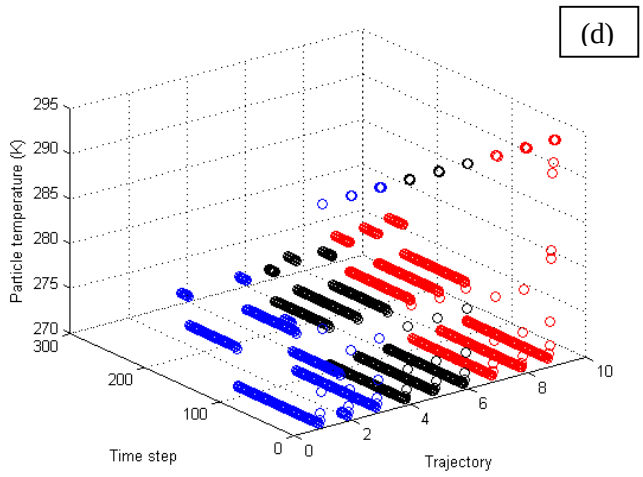

Figure 5.5. Particle tracking data, particle residence time (a), particle Reynolds number (b), particle time step size (c) and particle temperature (d).

From the figure 5.5a, it can be seen that the estimated value for maximum residence time in A.1 is reasonably safe, since most of the particles have a maximum residence time of less than $0.2\ s$ at the end of their trajectory. Figure 5.5b indicates that the assumption of Stokes regime in the equation of motion for the particles is satisfied ($Re_p \ll 1$). Particle time step size obtained during the calculations is shown in figure 5.5c, which shows that the time step for particle tracking is around one order of magnitude larger than the particle relaxation time (6×10^{-5} s). For the current degree of accuracy in the model, the chosen time step size works well without too much increase in the computational time. However, if more details like collision between particles, etc. are to be added to the model, the current time step size has to be modified. Figure 5.5d shows the variations of the particles' temperature. Regardless of the spatial position of the trajectory, all the particles are initially at the injection temperature. Once the evaporation starts, particles are in their wet bulb temperature. This corresponds to the region where particles are comparably large, but at the end of the trajectories, where the size of the particles becomes smaller and smaller, their temperature approaches the local temperature of the carrier phase.

5.3 Solution quality

In the following sections, the validity of the results from the model is analyzed by comparing them with experimental data. The quality of the solution is also discussed from numerical point of view.

5.3.1 Validation

Experimental measurements of the dryer include the typical flow rates in the system as well as the solvent concentration in the outflows. The latter has been particularly used in order to check if the model is able to predict the cut-off between the solvent concentration in the drying side and that of the exterior side of the column. Three different cases with ethanol as the solvent have been used, and the results of comparison are shown in figures 5.6 and 5.7.

The details of the three standard cases are included in table 5.2. The values for flow rates in table 5.2 are averaged values corresponding to steady state conditions of the dryer.

	Standard case		
Parameter	1	2	3
Injection flow rate ($\frac{kg}{s}$)	1.35e-08	1.28e-08	1.35e-08
Drying air flow rate ($\frac{L}{min}$)	41.13	45.87	41.17
Swirl flow rate ($\frac{L}{min}$)	0.45	0.48	0.40
Membrane effective diffusivity ($\frac{m^2}{s}$)	8.38E-06	8.38E-06	8.38E-06

Table 5.2. Details of the standard cases

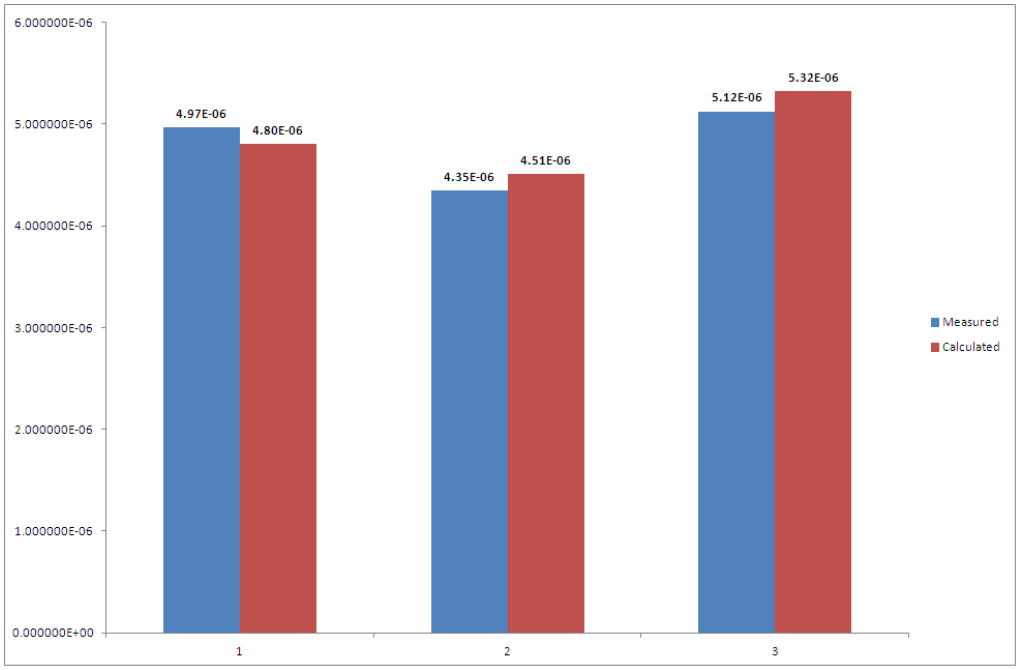

Figure 5.6. Comparison between the measured and calculated values of solvent concentration in the outflow of the exterior column

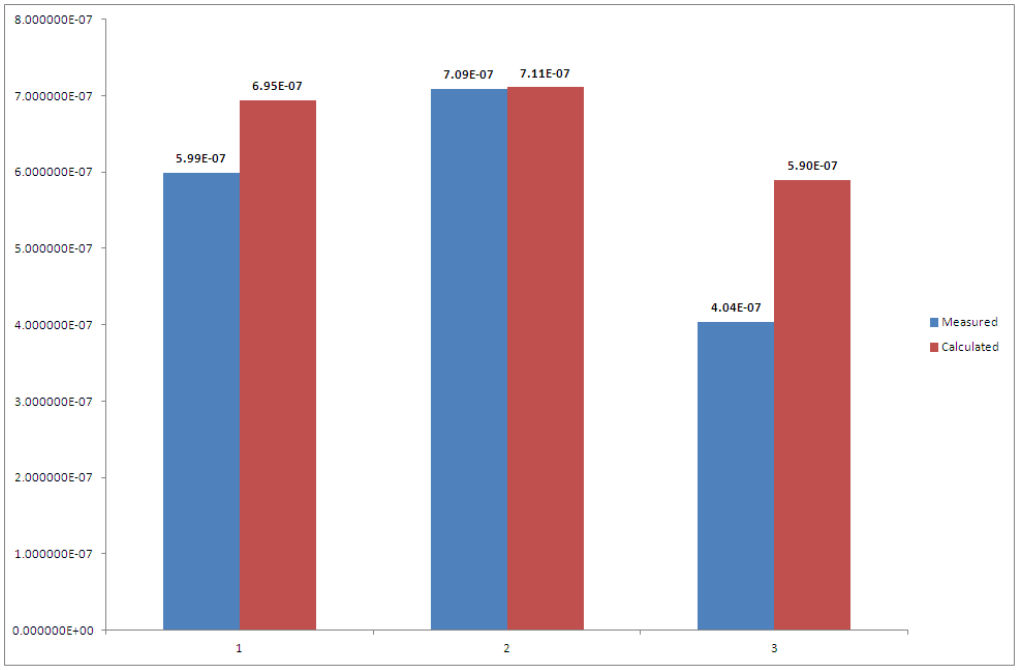

Figure 5.7. Comparison between the measured and calculated values of solvent concentration in the outflow of the drying column

As shown in figure 5.6, the model predictions for the outlet concentration of the exterior column are in firm agreement with the measurements. This is more or less valid about the first two cases in figure 5.7. However, some deviation is observed for the last case. Although the operating conditions for the third case is very much similar to the first one, the measured value of concentration in the drying column outflow is much lower than that of the first case, which can be considered to be a result of fluctuating swirl flow during the experiment. These fluctuations are shown and compared for the three standard cases in figure 5.8. As shown in figure 5.8, for the second case which the model gives the best prediction for, the swirl flow is fairly stable. For the first case, the overall flow is still stable but with some instantaneous fluctuations. However, for the third case, the swirl flow rate changes with time, and this introduces some error in the steady state value for concentration calculated from the experimental data. As will be discussed further, there is a direct connection between the swirl flow rate and the solvent concentration in the outflow, since the swirl flow rate affects both the residence time and concentration distribution in the column.

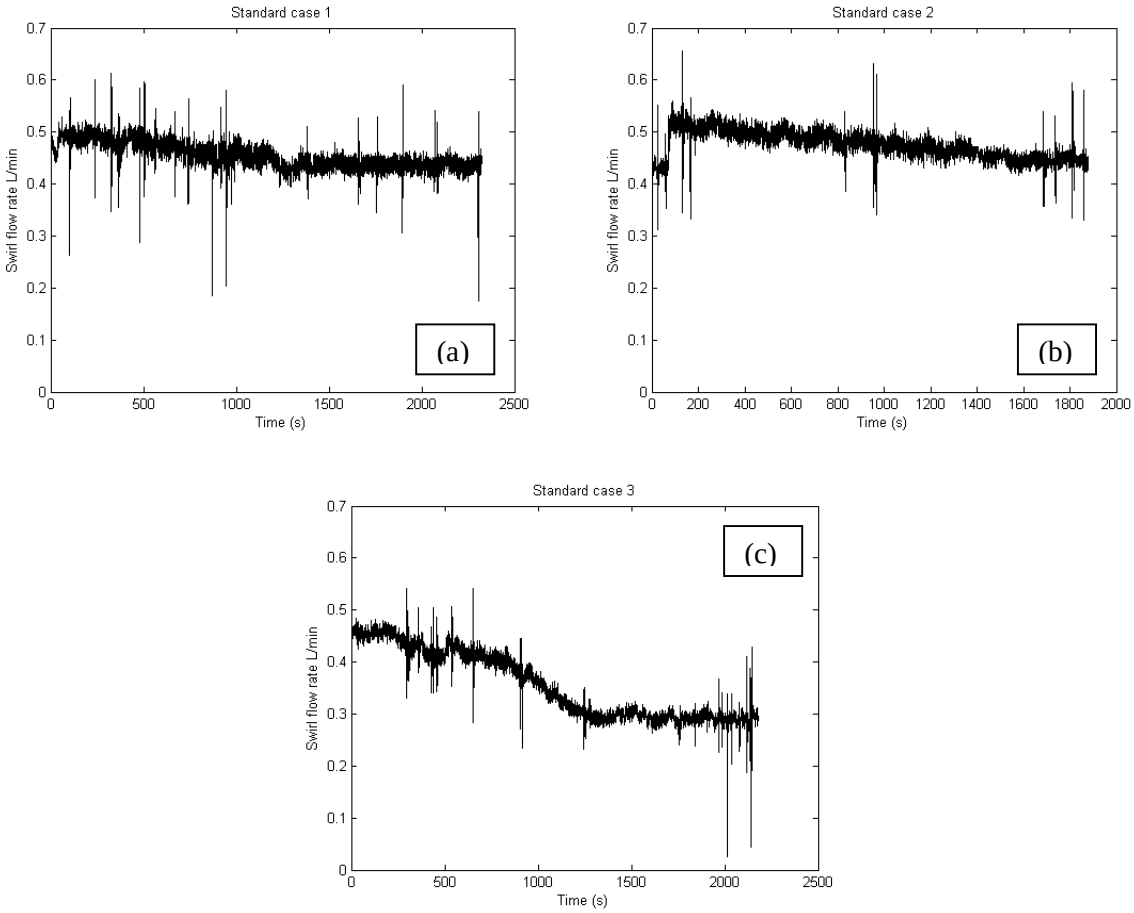

Figure 5.8. Swirl flow rate vs. time in standard cases 1 (a), 2 (b) and 3 (c)

5.3.2 Convergence

Convergence of the final solution has been controlled by monitoring specific quantities like concentration, velocity, etc. as well as the residuals. Practical experience shows that the convergence of the system of equations strongly depends on the energy equation. One reason is that the physical properties like latent heat of evaporation, diffusivity, density, etc. are temperature dependent. Another reason is that the equation of energy for the particulate phase is coupled to mass transfer from the particles, which form a stiff system of equations together. This decreases the stability of the solution and requires special care regarding the solution procedure. Figure 5.9 shows the convergence history of the monitored quantities.

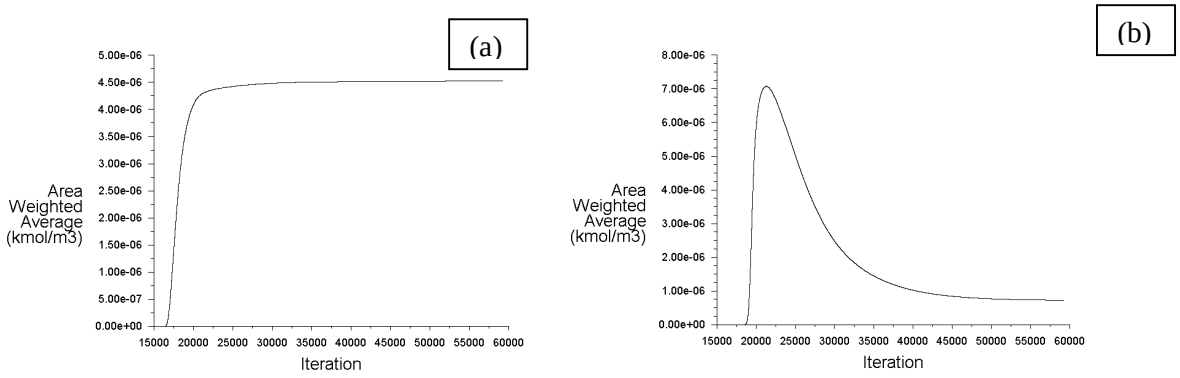

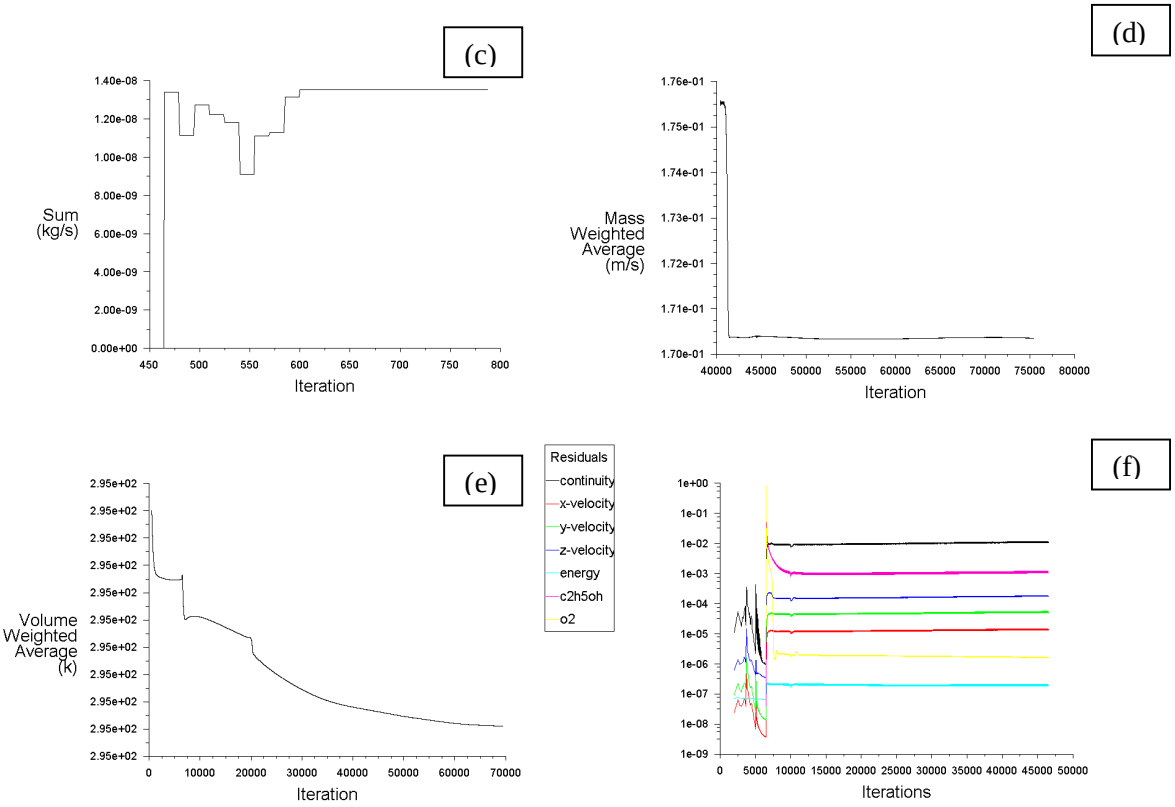

Figure 5.9. Convergence history of the monitored quantities, ethanol concentration in the exterior column outflow(a), ethanol concentration in the drying column outflow(b), discrete phase mass source(c), velocity in the outflows(d), temperature(e) and plot of residuals (f)

As shown in figure 23f, residuals are fairly stable, and except for the continuity equation (the black curve), their absolute value is fairly low.

5.3.3 Grid dependency

As discussed in 4.3.4.4, mass imbalance has to be monitored in order to make sure that a grid independent solution is obtained. Figure 5.10 shows a contour plot of mass imbalance in the system. Apart from the spray region, in the other parts a grid independent solution is obtained.

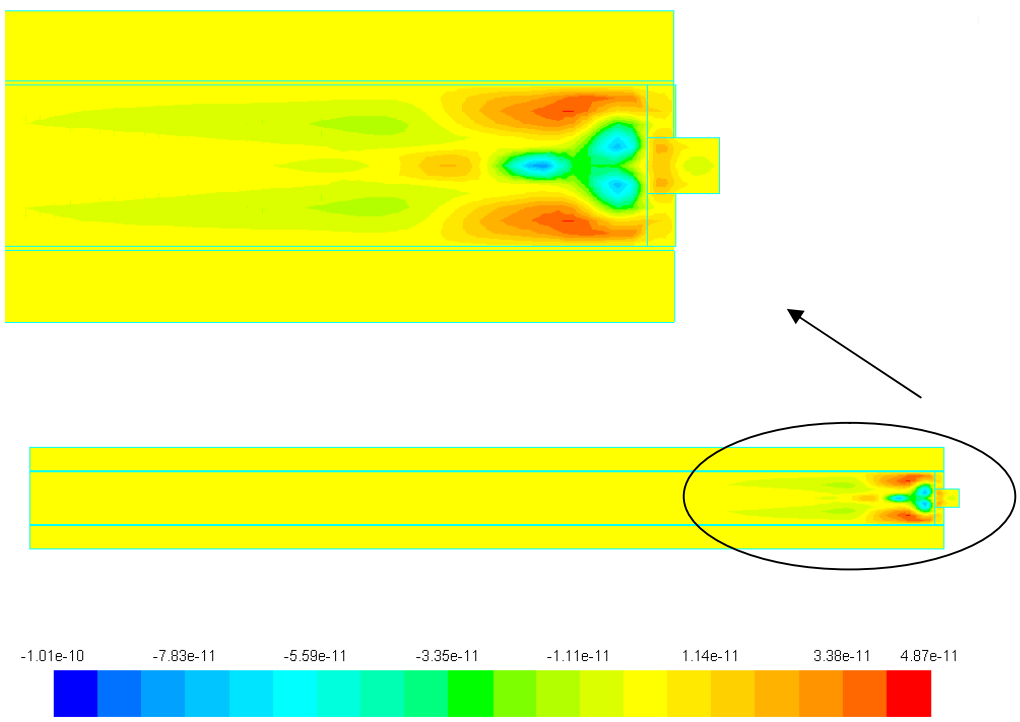

Figure 5.10. Contour plot of mass imbalance

One level of refinement has been applied to the spray region in order to eliminate the mass imbalance of the solution. Figure 5.11 shows the adapted region, where 720 cells were chosen for refinement, and each cell was then divided into one ‘parent’ and one ‘child’ cell. Previous refinement on the membrane is also depicted. Solution procedure has been performed on the refined mesh, and the quality of the solution in terms of mass imbalance has been analyzed. The result is shown in figure 5.12, which shows that mass imbalance has been significantly removed, and a reasonably grid-independent solution has been obtained.

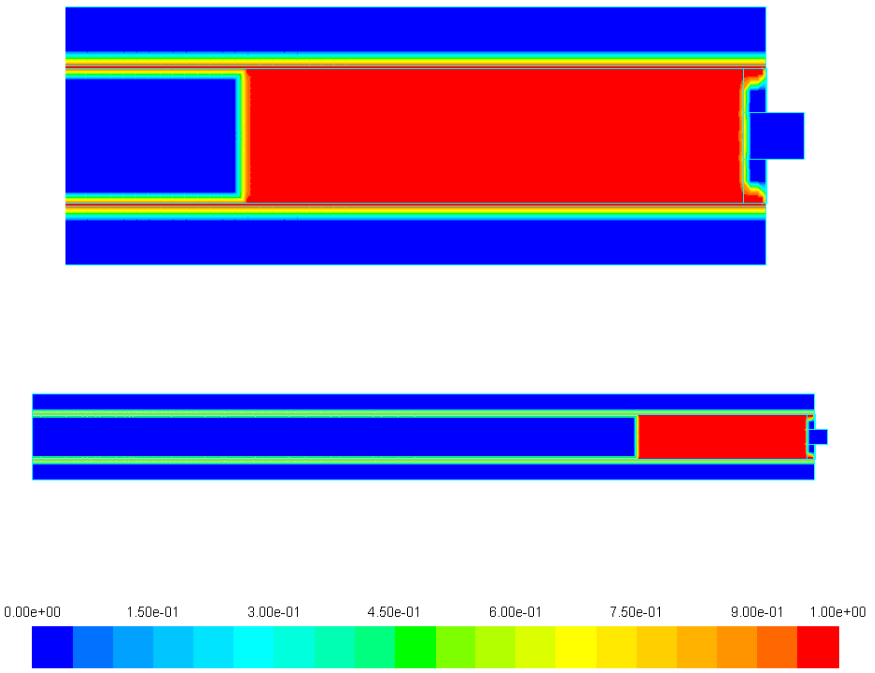

Figure 5.11. Adapted region, the color bar shows the number of cell children after refinement

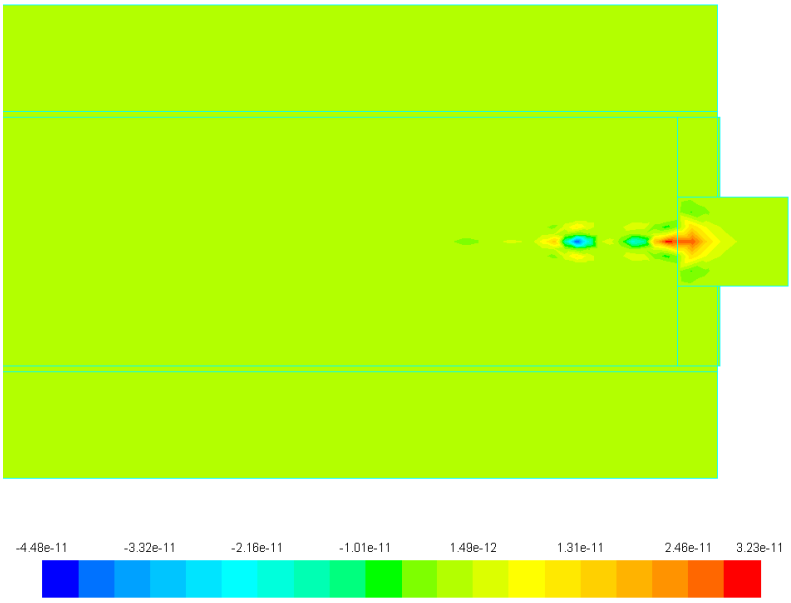

Figure 5.12. Contour plot of mass imbalance after refining the mesh

5.4 Design parameters

The following parameters have been reported as influencing design parameters in the literature, namely temperature and flow rate of the liquid spray, temperature and flow rate of the drying air and the parameters corresponding to the injection system, most importantly the initial droplet size [13]. Among these parameters, temperature is rather fixed, since spray drying of pharmaceuticals is desired to take place in room temperature. Injection parameters

in terms of initial size of the droplets are also inflexible, and so the parameters chosen for studying the behavior of the model are the flow rates as well as the diffusivity of the membrane. The effect of these parameters on the performance of the dryer is studied in the following sections.

5.4.1 Swirl flow rate

As discussed before, the swirl flow rate has a significant effect on the solvent concentration in the outflows. Further investigations reveal that there is a linear correlation between those parameters, such that by increasing the swirl flow rate, at constant injection and drying air flow rate, solvent concentration increases in the outlet of the drying column, while it decreases in the outlet of the exterior column. The results obtained from the model are shown in figure 5.13a and b for injection flow rate of $1.62 \times 10^{-7}\ \frac{kg}{s}$ and the drying air flow rate of $41.17\ \frac{L}{min}$.

Practical experience suggests that in order to prevent the risk of agglomeration in the final product solvent retention in the drying column outflow should be kept below 2%. At constant flow rates as described above, the amount of solvent retention as a function of swirl flow rate has been calculated as shown in figure 5.14.

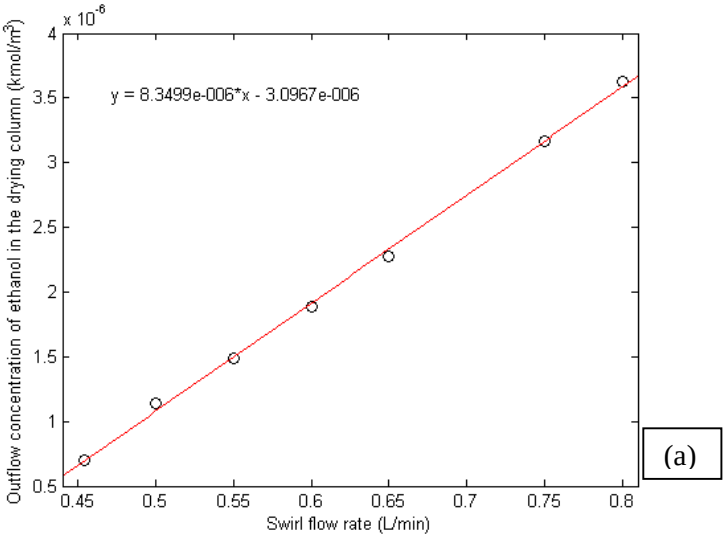

(a)

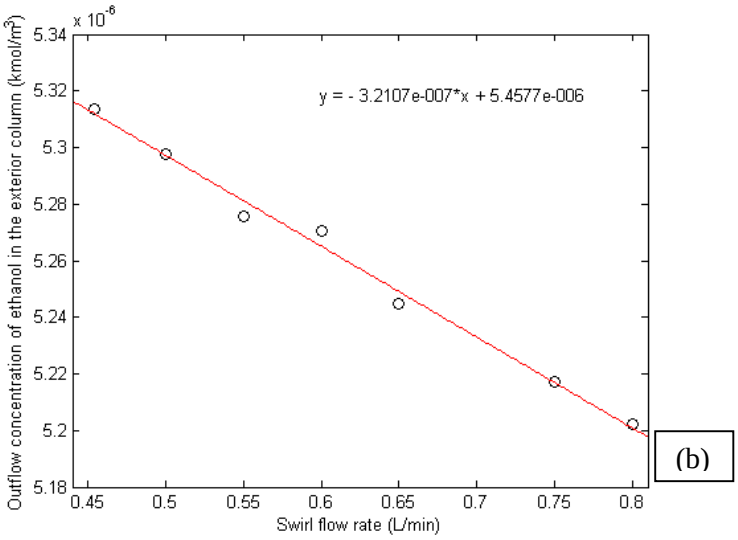

Figure 5.13. The impact of swirl flow rate on ethanol concentration in the outlet of the drying column (a) and the exterior column (b)

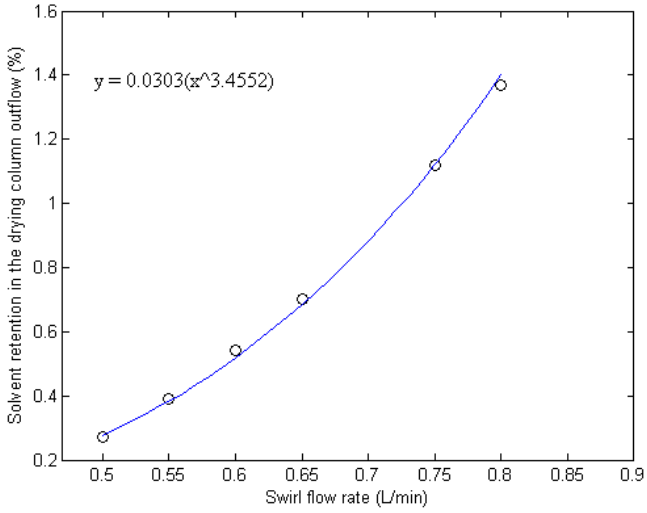

Figure 5.14. Solvent retention as a function of swirl flow rate

From the results shown in figure 5.14, it can be predicted that under the specified flow rates for injection and the drying air, the maximum possible swirl flow rate should be around $1.2\ \frac{L}{min}$.

5.4.2 Injection flow rate

Regarding the special mechanism of the nebulizer, it is not possible to directly manipulate the injection flow rate. The piezoelectric device works at a constant frequency, and hence the injection flow rate is also fixed. However, it is possible to use a control scheme to periodically turn the electric current on and off, such that a pause is introduced in between the injections,

which controls the overall flow rate over a certain period. The duration of the pause then determines the net flow rate. The nominal flow rate of the nebulizer is reported as $0.4\ \frac{mL}{min}$, but the dryer normally works at less than 5% of this value, i.e. around $0.012\ \frac{mL}{min}$.

The model has been used in order to predict the outflow concentrations for various injection flow rates, and the results are as shown in figure 5.15. Swirl flow rate as well as the drying air flow rate are according to standard cases, i.e. 0.48 and $45.87\ \frac{L}{min}$ respectively.

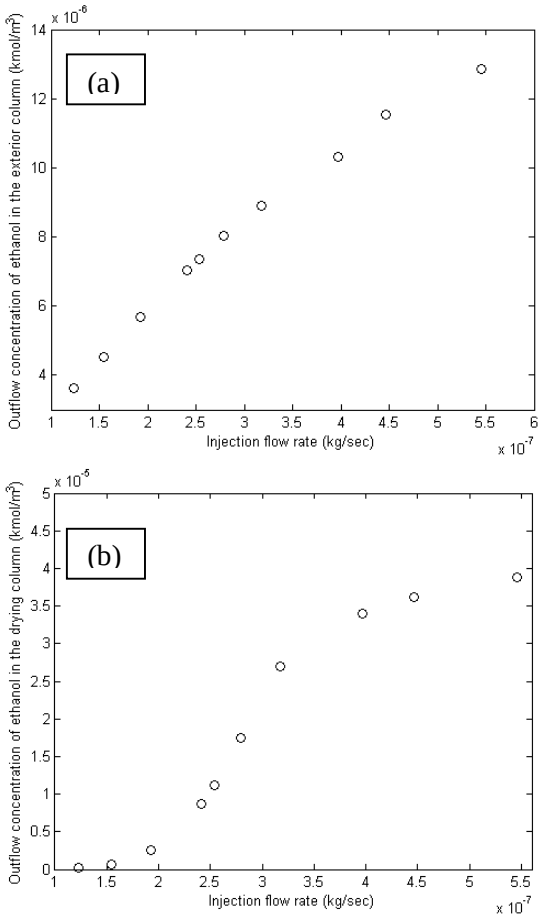

Figure 5.15. Ethanol concentration at the exterior column outflow (a) and drying column outflow (b) as a function of injection flow rate

As shown in figure 5.15, increasing the injection flow rate gives rise to the conditions where the interior column becomes saturated in ethanol. Under those conditions, it can be predicted that a large number of droplets fail to evaporate and will escape the column, which clearly should be avoided in operating the dryer. The injection flow rate which corresponds to saturation conditions is actually the nominal flow rate of the nebulizer, and this indicates that the current design of the column is not suitable to run at full injection capacity.

5.4.3 Effective diffusivity of the membrane

Simulation results show that the effective diffusivity of the membrane can have a significant effect on the performance of the dryer, since it actually determines the cut-off in the solvent concentration between the two outflow streams. These concentrations have been calculated for a number of diffusivity values for the membrane, and the results are as shown in figure 5.16. For each data point, the percentage of solvent retention has also been calculated and mentioned in figure 5.16c. As such, the lowest possible diffusivity which still keeps the solvent retention below 2% would be $2.55 \times 10^{-6} \frac{m^2}{s}$.

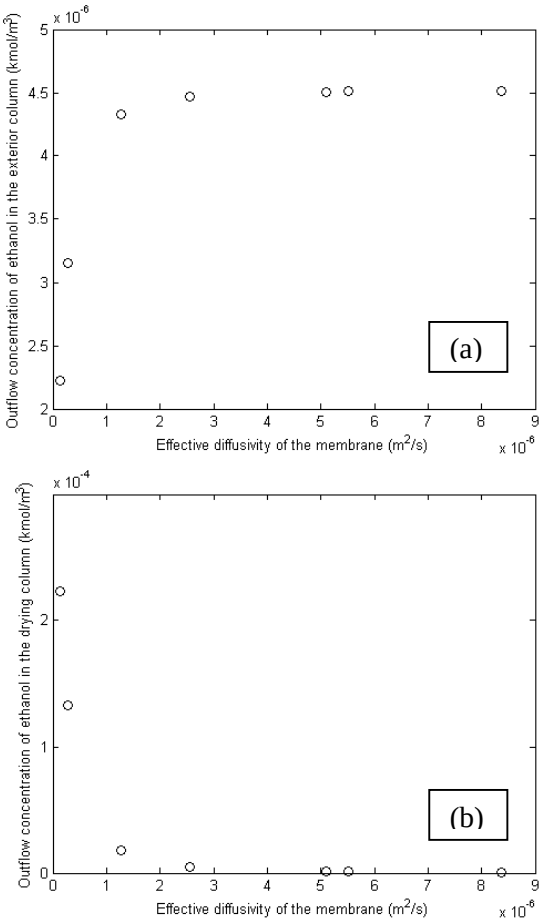

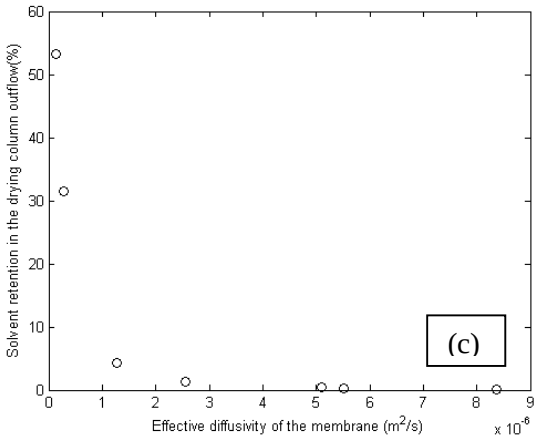

Figure 5.16. Ethanol concentration at exterior column outflow (a), drying column outflow (b), and percentage of solvent retention (c) as a function of effective diffusivity of the membrane

6. Development of an alternative design

An alternative design has been developed, in which the membrane as well as the support tube is removed, and the whole volume of the exterior column is made available for the aerosol to evaporate. This can be considered as expanding the diameter of the drying chamber and introducing a concurrent flow of the drying medium. The product should then be collected on a larger filter at the bottom of the column. In addition to a simpler characteristic of the equipment without any membrane separation step, another advantage of such a design is that a larger amount of drying medium can be used still in laminar regime, along with lower probability of wall deposition.

The effect of various injection flow rates has been studied for the new design in order to identify the maximum capacity that can be handled. The results are shown in figure 6.1; however, interpretation of these results requires additional experimental data about the equilibrium moisture content of the drug material as well as the maximum possible moisture content in the final product for which the risk of agglomeration is still negligible. Provided that these data are available, for each concentration in figure 6.1, an equilibrium moisture content in the solid product can be calculated, which can further be compared with the maximum allowed moisture content.

Figure 6.2 shows the contour plot of the cell Reynolds number in the new design, which guaranties a laminar regime in the flow field.

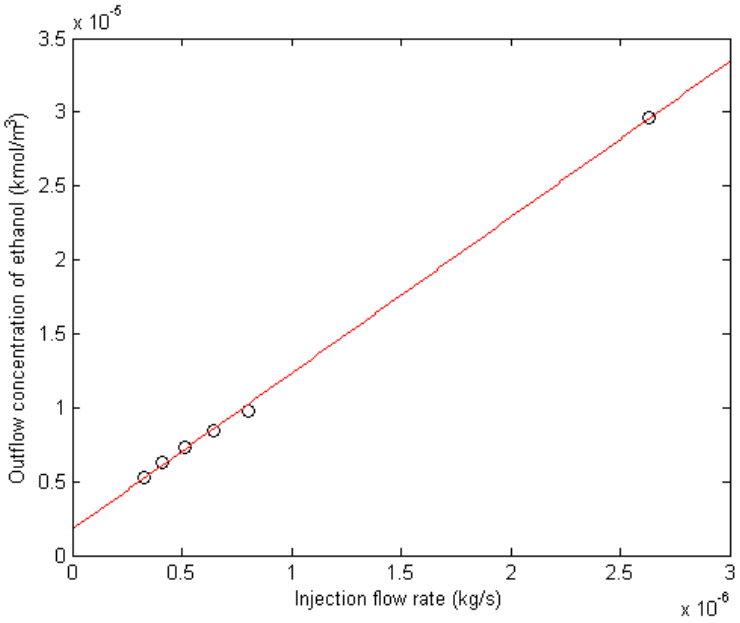

Figure 6.1. Outflow concentration of ethanol as a function of injection flow rate

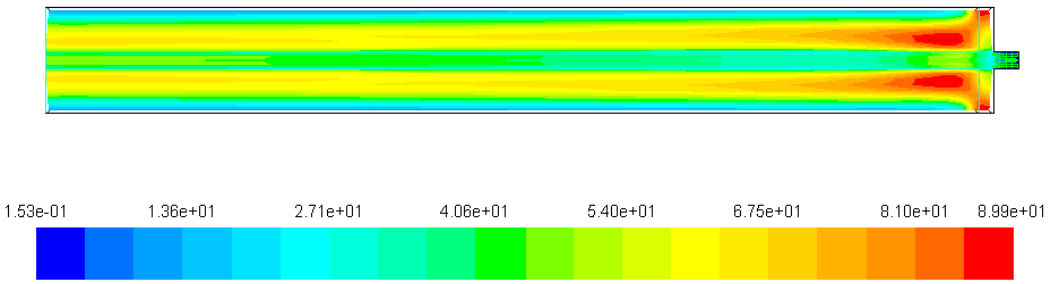

Figure 6.2. Contour plot of cell Reynolds number

Vector plot of the flow field is shown in figure 6.3, which indicates that effective swirl flow exists throughout the dryer, keeping the aerosol stream highly stabilized. This can significantly decrease the probability of wall deposition.

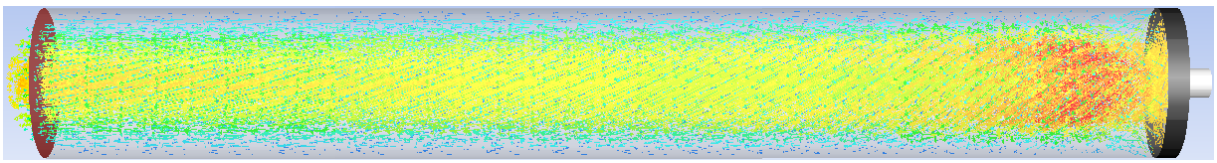

Figure 6.3. Vector plot of the flow field

Pathlines of tracer particles can also be used in order to better visualize the particle trajectories. One such graph is shown in figure 6.4, which indicates that the pathlines are fairly close to the centerline and the risk of wall deposition is minimized. It should be noted that real particles do not follow the whole pathline, since they evaporate at early stages of the dryer.

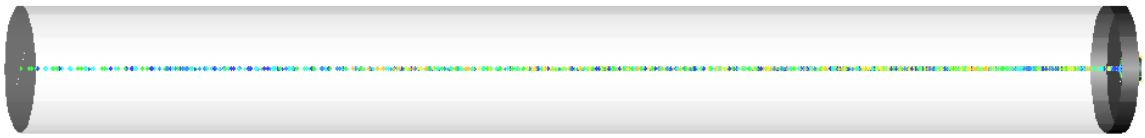

Figure 6.4. Pathlines of tracer particles

7. Conclusions

7.1 Summary

The novel design for spray drying of micron-sized particles has been studied, and a model for the system has been obtained based on the Eulerian-Lagrangian frame of reference. The model has been shown to be able to reproduce the experimental data from the dryer and hence can be used for design and prediction purposes. Parameter study has been done based on the derived model, which predicts the performance of the dryer under various operating conditions. The main advantage with the novel design is that a large amount of solvent material is removed so that the solvent concentration at the drying column outflow can be significantly reduced. Results from the model indicate that the novel design for spray dryer is capable of drying micronized droplets into fine powder effectively. Further investigations show a significantly low probability of wall deposition and particle agglomeration inside the drying chamber.

Furthermore, the performance of the dryer has been shown to be sensitive to injection flow rate and the effective diffusivity of the membrane. Above a certain limit for injection flow rate, the dryer becomes saturated, and solvent concentration starts to rapidly increase in the drying column outflow. The operating range for effective diffusivity of the membrane is rather tight, and the use of membrane material with very low diffusivities should be avoided.

Outflow concentrations of the solvent material have been shown to linearly depend on swirl flow rate, mainly due to the fact that the aforementioned parameter directly influences the residence time distribution inside the dryer.

An alternative design has been developed and studied with the same model. The membrane system has been excluded in the new design such that larger amounts of the drying medium can be made available for the aerosol. Numerical results have been obtained for the proposed design; however, it requires additional sets of experimental data in order to judge its performance.

7.2 Potentials for future work

The current study focused on the drying process of pure solvent only. In order to better consider the performance of the dryer in terms of wall deposition and the quality of the final product, additional effort is required to upgrade the current model to one which includes the effects of solid material as well. Formation of the solid phase will both affect the drying rate of the particles and their trajectories. Diffusion of the vapor phase through the porous structure of the crystals should be accounted for, and hence the model should be supported with suitable drying kinetic data of the drug material. From the fluid dynamic point of view, in contrast with the case of pure solvent where the droplets evaporate in the early stages of drying, solid particles will follow their trajectories throughout the column, and hence wall deposition should be studied in more detail. Equation of motion for the solid particles should be coupled with the drying state of the material in order to obtain a better prediction for wall deposition. Regarding the quality of the final product, additional experimental data including the studies of equilibrium moisture content and the maximum allowable moisture content in the final product might also be required.

8. Nomenclature

$\boldsymbol{A}$	Control surface area $[m^2]$
A_d	Droplet surface area $[m^2\ ]$
C_n	Concentration of species n $[\frac{mol}{m^3}]$
C_p	Heat capacity $[\frac{J}{kg.K}]$
$d,\ d_p$	Particle diameter $[m]$
$D,\ D_n$	Molecular diffusivity $[\frac{m^2}{s}]$
D_{ij}	Prescribed parameter for porous zone definition $[\frac{1}{m^2}]$
$D_{ei},\ D_{eff}$	Effective diffusivity $[\frac{m^2}{s}]$
E	Total energy of a closed system $[J]$
$\boldsymbol{F}$	Force $[N]$
F_i	Total force acting on a closed system $[N]$
g_i	Body force in the i direction per unit volume $[\frac{N}{m^3}]$
$\boldsymbol{g}_i$	Gravitational acceleration $[\frac{m}{s^2}]$
k	Thermal conductivity $[\frac{W}{m\ .K}]$

M	Total mass of a closed system $[kg]$
$\dot{M}_{p,j}$	Mass flow rate of particles on trajectory j $[\frac{kg}{s}]$
m	Mass $[kg]$
$m_{p,j}$	Initial mass of the particles on trajectory j $[kg]$
Δm	Porous zone thickness $[m]$
N_i	Molar flux of species i $[\frac{mol}{m^2.s}]$
$\dot{N}_{p,j}$	Number flow rate of particles on trajectory j $[\frac{1}{s}]$
n_j	Unit normal vector
Nu	Nusselt number
P	Pressure $[Pa]$
P_{i0}, P_{iL}	Partial pressure of species i $[Pa]$
P_{Mi}	Permeability $[\frac{mol}{Pa.m.s}]$
Pr	Prandtl number
$\dot{Q}$	Net heat transfer rate to a closed system $[W]$
$\dot{Q}_d$	Heat transfer rate to the droplet $[W]$
R	Universal ideal gas law constant
Re	Reynolds number
S	Control surface area $[m^2]$
S_i	Momentum source term $[\frac{N}{m^3}]$
S_m	Mass source term $[\frac{kg}{m^3.s}]$
S_n	Concentration source term $[\frac{mol}{m^3.s}]$
S_P	Momentum source term $[\frac{N}{kg}]$
S_T	Energy source term $[\frac{W}{m^3}]$
Sc	Schmidt number

Sh	Sherwood number
St	Stokes number
$T,\ T_\infty,\ T_s$	Temperature $[K]$
T_w	Wet-bulb temperature $[K]$
t	Time $[s]$
Δt	Time interval (used for time marching) $[s]$
$\boldsymbol{U}$	Velocity $[\frac{m}{s}]$
$u_i,\ U_i,\ U_j$	Velocity in i, j direction $[\frac{m}{s}]$
$\boldsymbol{u}_p$	Particle velocity $[\frac{m}{s}]$
$V\ , V_j,\ \boldsymbol{V}$	Velocity $[\frac{m}{s}]$
$\dot{W}$	Net rate of work done by a closed system $[W]$
$\boldsymbol{w}$	Velocity $[\frac{m}{s}]$
X_s, X_∞	Mass fraction
x	Spatial position of the cell/face centroid
$x_i,\ x_j$	i, j component of the coordinate system
α_d	Volume fraction of the dispersed phase
$\delta V_d\ , \delta V$	Volume $[m^3]$
ϵ	Porosity
λ	Latent heat of evaporation $[\frac{J}{kg}]$
μ	Viscosity $[Pa.s]$
μ_f	Fluid viscosity $[Pa.s]$
ϕ	Conserved property in the transport equations
ρ, ρ_s	Density $[\frac{kg}{m^3}]$
ρ_p	Particle density $[\frac{kg}{m^3}]$
σ_{ij}	Shear stress $[Pa]$

τ	Tortuosity
τ_f	Fluid flow time scale $[s]$
τ_{ji}, τ_{kj}	Shear stress $[Pa]$
τ_{xp}	Particle relaxation time $[s]$

Appendix

A.1 Volume fraction of the dispersed phase

For the extreme case discussed in 3.2, the largest α_d is calculated as follows.

$$V_d = \dot{Q}_i \times \tau_r \qquad (A1)$$

$\dot{Q}_i$ and τ_r are volumetric flow rate of injection and average residence time respectively. $\dot{Q}_i$for a periodic segment is $1.716 \times 10^{-11}\ \frac{m^3}{s}$ for standard cases (for which experimental data is available). Exact value of the residence time is not known a priori, but a maximum value is obtained from an average cell dimension and the minimum velocity for traversing the cell:

$$\tau_{r,max} = \frac{cell\ dimension\ (m)}{u_{min}\ (\frac{m}{s})} \qquad (A2)$$

Average cell dimension in the injection region is around $0.0024\ (m)$, and the minimum velocity at that region is estimated from the continuous phase velocity, knowing that particles move more or less with the same velocity as that of the continuous phase:

$u_{min} = 9.23 \times 10^{-3}\ \frac{m}{s} \Rightarrow$

$\tau_{r,max} = 0.26\ s \Rightarrow$

$V_d = 1.716 \times 10^{-11} \times 0.26 = 4.462 \times 10^{-12}\ m^3 \Rightarrow$

$\alpha_{d,max} = \frac{4.462 \times 10^{-12}}{4 \times 10^{-9}} \times 100 = 0.1\%$

A.2 User's Defined Function

```
/************************************************************
   UDF for calculating diffusivity of the mixture components
************************************************************/

#include <udf.h>

enum{c2h5oh,o2,n2};
DEFINE_DIFFUSIVITY(Deff,c,t,i)
{
double Deff,T;
int zone_ID = THREAD_ID(t);
T=C_T(c,t);
if(i==0)              // EtOH
{
                      if (zone_ID == 14 || zone_ID == 11 || zone_ID == 12)
                      {
                      Deff=8.378406e-6;
                      }
                      else
                      {
                      Deff=3.238387e-9*pow(T,1.5);       //Diffusivity from the kinetic theory
                      }
 }
else if(i==1)       //O2
{
                      if (zone_ID == 14 || zone_ID == 11 || zone_ID == 12)
                      {
                      Deff=1e-15;                  //No diffusion through the membrane
                      }
                      else
                      {
                      Deff=4.054569e-9*pow(T,1.5);       //Diffusivity from the kinetic theory
                      }
}
else                 //N2
{
                      if (zone_ID == 14 || zone_ID == 11 || zone_ID == 12)
                      {
                      Deff=1e-15;                  //No diffusion through the membrane
                      }
                      else
                      {
                      Deff=4.054571e-9*pow(T,1.5);       //Diffusivity from kinetic theory
                      }
}
                      return Deff;
}
/************************************************************
    Soheil Soltani 25 April 2012
************************************************************/
```

References

1. Lee, S.H., et al., *Nano spray drying: A novel method for preparing protein nanoparticles for protein therapy.* International Journal of Pharmaceutics, 2011. **403**(1-2): p. 192-200.
2. Gerde, P., Sjöberg, C.O. and Acevedo, F., *The LaminarPace Spray Dryer: Producing Small Portions of Fine Powders at Ambient Temperature in High Yields.* Respiratory Drug Delivery, 2010. **2**: p. 605-608.
3. Blei, S. and M. Sommerfeld, *CFD in Drying Technology – Spray-Dryer Simulation*, in *Modern Drying Technology*. 2007, Wiley-VCH Verlag GmbH & Co. KGaA. p. 155-208.
4. Crowe, C.T., M.P. Sharma, and D.E. Stock, *Particle-Source in Cell (Psi-Cell) Model for Gas-Droplet Flows.* Journal of Fluids Engineering-Transactions of the Asme, 1977. **99**(2): p. 325-332.
5. YouTube. *http://www.youtube.com/watch?v=1lA_SSScMeE*. 2010.
6. Aerogen, L., *Aeroneb®Pro Micropump Nebulizer Instruction Manual*. 2011, AL: Galway.
7. Gerde, P., et al., *A novel method to aerosolize powder for short inhalation exposures at high concentrations: Isolated rat lungs exposed to respirable diesel soot.* Inhalation Toxicology, 2004. **16**(1): p. 45-52.
8. Rubow, K.L., et al., *A Personal Cascade Impactor - Design, Evaluation and Calibration.* American Industrial Hygiene Association Journal, 1987. **48**(6): p. 532-538.
9. Langrish, T.A.G. and D.F. Fletcher, *Spray drying of food ingredients and applications of CFD in spray drying.* Chemical Engineering and Processing, 2001. **40**(4): p. 345-354.
10. Langrish, T.A.G., *Multi-scale mathematical modelling of spray dryers.* Journal of Food Engineering, 2009. **93**(2): p. 218-228.
11. Crowe, C.T., *Multiphase flows with droplets and particles*. 2nd ed. 2012, Boca Raton: CRC Press. xv, 494 p.
12. Jakobsen, H.A., *Chemical reactor modeling : multiphase reactive flows*. 2008, Berlin: Springer. lii, 1244 p.
13. Gauvin, W.H., S. Katta, and F.H. Knelman, *Drop trajectory predictions and their importance in the design of spray dryers.* International Journal of Multiphase Flow, 1975. **1**(6): p. 793-816.
14. Maxey, M.R. and J.J. Riley, *Equation of Motion for a Small Rigid Sphere in a Nonuniform Flow.* Physics of Fluids, 1983. **26**(4): p. 883-889.
15. Crowe, C.T., *Modeling spray-air contact in spray-drying systems.* Advances in drying, 1980. **1**.
16. Seader, J.D. and E.J. Henley, *Separation process principles*. 2nd ed. 2006, Hoboken, N.J.: Wiley. xxxiv, 756 p.
17. Zbicinski, I., *Development and Experimental-Verification of Momentum, Heat and Mass-Transfer Model in Spray-Drying.* Chemical Engineering Journal and the Biochemical Engineering Journal, 1995. **58**(2): p. 123-133.
18. *ANSYS FLUENT User's Guide*. 2011, ANSYS Inc.
19. Andersson, B., *Computational fluid dynamics for engineers*. 2012, Cambridge ; New York: Cambridge University Press. xi, 189 p.
20. Dou, H.S., B.C. Khoo, and H.M. Tsai, *Determining the critical condition for turbulent transition in a full-developed annulus flow.* Journal of Petroleum Science and Engineering, 2010. **73**(1-2): p. 41-47.
21. Gouesbet, G. and A. Berlemont, *Eulerian and Lagrangian approaches for predicting the behaviour of discrete particles in turbulent flows.* Progress in Energy and Combustion Science, 1999. **25**(2): p. 133-159.
22. Eslamian, M. and N. Ashgriz, *Effect of atomization method on the morphology of spray-generated particles.* Journal of Engineering Materials and Technology-Transactions of the Asme, 2007. **129**(1): p. 130-142.

23. Arulmuthu, E.R., et al., *Studies on aerosol delivery of plasmid DNA using a mesh Nebulizer.* Biotechnology and Bioengineering, 2007. **98**(5): p. 939-955.
24. Dutta, B.K., *Principles of mass transfer and separation processes*. 2007, New Delhi: Prentice Hall of India